Twinfilin uncaps filament barbed ends to promote turnover of lamellipodial actin networks

Hakala, Markku

2021-02-08

Hakala , M , Wioland , H , Tolonen , M , Kotila , T , Jegou , A , Romet-Lemonne , G & Lappalainen , P 2021 , ' Twinfilin uncaps filament barbed ends to promote turnover of lamellipodial actin networks ' , Nature Cell Biology , vol. 23 , no. 2 , pp. 147-+ . https://doi.org/10.1038/s41556-020-00

http://hdl.handle.net/10138/337901
https://doi.org/10.1038/s41556-020-00629-y

other
acceptedVersion

Twinfilin uncaps filament barbed ends to promote turnover of lamellipodial actin networks

Markku Hakala[1], Hugo Wioland[2], Mari Tolonen[1], Tommi Kotila[1], Antoine Jegou[2], Guillaume Romet-Lemonne[2], Pekka Lappalainen[1]*

1) Institute of Biotechnology and Helsinki Institute of Life Sciences, University of Helsinki, P.O. Box 56, 00014 Helsinki, Finland

2) Université de Paris, CNRS, Institut Jacques Monod, F-75006 Paris, France

*) To whom correspondence should be addressed: Institute of Biotechnology, P. O. Box 56, FI-00014 University of Helsinki, Finland. Tel.: 358-50-415-5433; E-mail: pekka.lappalainen@helsinki.fi.

ABSTRACT

Coordinated polymerization of actin filaments provides force for cell migration, morphogenesis, and endocytosis. Capping Protein (CP) is central regulator of actin dynamics in all eukaryotes. It binds actin filament (F-actin) barbed ends with high affinity and slow dissociation kinetics to prevent filament polymerization and depolymerization. In cells, however, CP displays remarkably rapid dynamics within F-actin networks, but the underlying mechanism has remained enigmatic. We report that a conserved cytoskeletal regulator, twinfilin, is responsible for CP's rapid dynamics and specific localization in cells. Depletion of twinfilin led to stable association of CP with cellular F-actin arrays, and to its retrograde movement throughout leading-edge lamellipodium. These were accompanied by diminished F-actin turnover rates. *In vitro* single filament imaging approaches revealed that twinfilin directly promotes dissociation of CP from filament barbed ends, while allowing subsequent filament depolymerization. These results uncover a bipartite mechanism that controls how actin cytoskeleton-mediated forces are generated in cells.

Actin filament (F-actin) polymerization generates pushing force, which drives lamellipodia protrusion at the leading edge of migrating cells and contributes to the formation of plasma membrane invaginations in endocytosis[1–4]. A large array of actin-binding proteins regulates the dynamics and organization of actin filaments in cells, but only few (<10) are conserved in evolution from protozoan parasites to animals[5]. Among these 'core' actin-binding proteins are the heterodimeric Capping Protein (CP) and twinfilin.

Generation of membrane protrusions requires that a subset of actin filament barbed ends is capped to funnel the assembly-competent actin monomers to a limited number of growing barbed ends[6–8]. CP is the most prominent actin filament barbed end capper in most cell types[9,10]. It is an essential component of *in vitro* reconstituted actin-based motility[11] and actin-based processes such as cell migration[12–18]. CP also controls the length and density of branches within actin filament networks nucleated by the Arp2/3 complex[19].

Activity of CP is controlled by several proteins[9,10]. V-1/myotrophin binds and sequesters CP with nanomolar affinity and inhibits its capping activity[20–23]. The capping protein interaction (CPI)-motif-containing proteins, such as CARMILs (capping protein, Arp2/3 and myosin-I linker protein)[24], interact with CP to reduce its affinity to both actin filament barbed ends[25–27] and to V-1[22,25,28]. Depletion of CARMILs and other CPI motif-containing proteins disrupts the subcellular localization of CP[29–33]. Thus, it was suggested that CPI-motif proteins activate CP near the plasma membrane by competing with V-1[22].

CP binds actin filament barbed ends with sub-nanomolar affinity and displays very slow dissociation kinetics *in vitro* (K_{off}-rate 0.4-0.5 x 10^{-3} s^{-1})[34–36]. However, its turnover in cells is orders of magnitude faster (K_{off}-rate 0.1-0.58 s^{-1})[37,38] and its localization is restricted to the very distal edge in lamellipodia of motile cells[14,22,37]. The discrepancy between biochemical and cellular experiments suggests that

additional factors regulate uncapping of CP-capped barbed ends. Both CARMIL and ADF/cofilin can enhance uncapping of filament barbed ends *in vitro*, but through different mechanisms. ADF/cofilin decorates actin filaments, and when the ADF/cofilin segment reaches the filament barbed end, it increases the dissociation rate of CP (K_{off}-rate 6 x 10^{-3} s^{-1})[35]. Dissociation of CP is followed by disassembly of the ADF/cofilin-decorated actin filament from the barbed end[35]. Stabilization of actin filaments by jasplakinolide or through over-expression of LIM kinase resulted in diminished CP speckle lifetime in lamellipodia of fibroblasts, providing evidence that ADF/cofilin-mediated F-actin disassembly enhances CP-dynamics[38]. CARMIL enhances CP dissociation from barbed ends by interacting with CP and decreasing its affinity to barbed ends (K_{off}-rate ~ 0.07 s^{-1}) through an allosteric mechanism[25,39]. Whether the rapid dynamics of CP within dendritic actin filament networks relies solely on actin filament severing and depolymerization, or if direct filament uncapping also contributes to CP dynamics has remained elusive.

Twinfilin is composed of two actin-binding ADF-H (actin-depolymerization factor homology) domains, followed by a CPI-motif containing C-terminal tail[40], which binds CP and phosphoinositides[41–43]. Twinfilin sequesters actin monomers[44–46], caps filament barbed ends[47] and accelerates actin filament depolymerization *in vitro* in concert with cyclase-associated protein (Srv/CAP)[48,49]. Depletion of twinfilin in *Drosophila* S2 cells leads to the expansion of the lamellipodium, and budding yeast cells lacking twinfilin display defects in the turnover of endocytic actin patches[15,44]. However, the precise mechanisms by which twinfilin contributes to these and various other actin-dependent processes in cells[50–53] has remained enigmatic. The presence of two twinfilin genes in mammals, that encode the ubiquitously expressed twinfilin-1 and twinfilin-2a, and a muscle specific isoform twinfilin-2b[40,54], further complicates the analysis of twinfilin's functions in cells.

Here, we reveal that the correct localization and rapid dynamics of CP in animal cells are dependent on twinfilin. Measurements of single actin filament dynamics *in vitro* demonstrated that CP rapidly

dissociates from the actin filament barbed ends in the presence of twinfilin. These results explain how CP undergoes rapid turnover at actin filament barbed ends in cells.

RESULTS

Depletion of twinfilin results in abnormal actin filament accumulation and lamellipodial dynamics

To reveal the role of twinfilin in actin dynamics in mammalian cells, we generated twinfilin-1, twinfilin-2, and twinfilin-1/twinfilin-2 double knockout (hereafter referred to as twf1/twf2-KO) mouse melanoma B16-F1 cell-lines (Extended Data Fig. 1). Inactivation of either *twinfilin-1* or *twinfilin-2* gene did not result in drastic defects in the actin cytoskeleton (Figure 1 a-b), suggesting that they are functionally redundant. Accordingly, twf1/twf2-KO cells exhibited more severe abnormalities in actin-dependent processes. In comparison to wild-type cells, lamellipodia of twf1/twf2-KO cells were less smooth (Figure 1a). The twf1/twf2-KO cells also appeared to display a small increase in F-actin levels, while the total levels of actin and central regulators of actin dynamics appeared unaltered (Figure 1b, d, Extented Data Fig. 2).

We also noticed a significant increase in the intensities of both F-actin and the Arp2/3 complex at the leading edge lamellipodia in twf1/twf2-KO cells, suggesting that the F-actin network is more dense in twinfilin-deficient cells (Figure 1 e-f). Transient expression of EGFP-twinfilin-1 rescued increased F-actin levels in twf1/twf2-KO cells, suggesting that they do not result from off-target effects (Figure 1c-f). Increased F-actin amounts in lamellipodia in twf1/twf2-KO cells were accompanied by the decrease in the velocity of lamellipodia protrusions (Figure 1g, Supplementary video 1) and random cell migration in a two-dimensional environment (Figure 1h, Supplementary video 2).

Twinfilin-1 co-localizes with actin in transferrin-positive endosomes[47]. By labelling endosomes with fluorescent transferrin, we observed that F-actin accumulated at transferrin-positive punctae especially at the perinuclear region of twf1/twf2-KO cells (Extended Data Fig. 3a-b). High-content analysis revealed a small increase in F-actin intensity on transferrin positive endosomes of twf1/twf2-KO cells compared to wild-type cells (Extended Data Fig. 3c).

Twinfilin promotes actin filament turnover in the lamellipodium

To address if abnormal accumulation of actin filaments in twf1/twf2-KO cells is due to altered actin dynamics, we performed a fluorescence-recovery-after-photobleaching (FRAP) assay on cells expressing EGFP-β-actin. This assay revealed that the F-actin network assembly rate relative to the lamellipodium tip was diminished in twf1/twf2-KO cells compared to wild-type B16-F1 cells (Figure 2a-d, Supplementary video 3). The slower F-actin assembly rate at the lamellipodia is consistent with the decreased lamellipodial protrusion velocity in twinfilin-deficient cells (Figure 1f).

We next examined F-actin dynamics in lamellipodia by a photoactivation approach. For this purpose, we co-transfected wild-type and twf1/twf2-KO cells with plasmids expressing photoactivatable PA-GFP-β-actin and Cherry-LifeAc (as a marker for lamellipodial actin filaments). Significant decrease in the rate of PA-GFP-actin fluorescence decay was observed at the lamellipodia of twf1/twf2-KO cells compared to wild-type cells. This phenotype could be rescued by expressing mCherry-TWF-1 (Figure 2e-f, Supplementary video 4). These results suggest that actin filament depolymerization rates are diminished at the lamellipodia of twf1/twf2 knockout cells, because earlier studies proposed that decay of actin fluorescence in a similar setting is proportional to the rate of actin filament disassembly[55–57]. However, since the photoactivation assay cannot detect the turnover of individual actin filaments, and because both actin filament assembly and disassembly are mechanistically linked to each other in cells, the precise effect of twinfilin on actin dynamics in cells cannot be determined by these approaches.

Effects of twinfilin on actin filament barbed end polymerization and depolymerization

We next analyzed the effect of mouse twinfilin-1 on the dynamics of single actin filaments *in vitro* using microfluidics[58,59] (Figure 3a). Importantly, we detected a similar rate of barbed end depolymerization of bare ADP-actin filaments (~10 subunits/s) as in previous studies by bulk, single filament, and electron microscopy assays[60–63] (Figure 3b). Surprisingly, addition of twinfilin-1 did not accelerate filament barbed end depolymerization as previously reported[48,49]. Instead, we observed a concentration-dependent decrease in filament barbed end depolymerization rate that plateaued to the level of ~6 subunits/s at saturating twinfilin-1 concentration (Figure 3b). We hypothesize that the difference between our results and earlier open chamber experiments[48,49] may result from pauses that occur during depolymerization of surface-anchored filaments in open chamber experiments[64]. These pauses are due at least in part to multiple surface-anchoring points. When excluding pauses from the analysis, we found that open chamber actin depolymerization experiments replicated the results from the single filament microfluidics experiments (Extended Data Fig. 4a-c). Moreover, a fluorometric assay on actin filaments capped at their pointed ends by Tmod1 demonstrated that filaments depolymerized from their barbed ends more slowly in the presence of full-length mouse twinfilin-1 as compared to its C-terminal ADF-H domain, which only sequesters actin monomers[65] (Extended Data Fig. 4d). Finally, we tested if cyclase-associated-protein would affect actin filament barbed end depolymerization rates by twinfilin[48,49]. Similar to our observations on twinfilin only, addition of the N-terminal half of mouse cyclase-associated-protein 1 (CAP1) did not lead to enhanced barbed end depolymerization (Figure 3c).

To examine if twinfilin prevents actin filament polymerization at barbed ends, as suggested by earlier experiments[47], the assay was performed under assembly promoting conditions in the presence of various profilin-actin concentrations, and by varying the concentration of twinfilin-1 (Figure 3d-e).

Consistent with earlier results[47], increasing the concentration of twinfilin-1 gradually slowed down actin filament barbed end polymerization. The amplitude of this effect at low twinfilin-1 concentrations cannot be accounted for by a one-to-one G-actin sequestration alone (*e.g.* in Figure 3e, adding 1 μM twinfilin-1 to 4 μM actin and 4 μM profilin reduces the elongation rate 3-fold, similar to[47,65]), indicating that twinfilin interacts directly with the filament barbed end. No pauses in the elongation were detected, suggesting that there was no prolonged capping of barbed ends by twinfilin. At high twinfilin-1 concentrations, filaments depolymerized and reached the rate of ~6 subunits/s that was also measured in the absence of G-actin (Figure 3e). These data suggest that twinfilin sequesters actin monomers and transiently associates with actin filament barbed ends to inhibit filament polymerization, while allowing their depolymerization with a rate of approximately 6 subunits/s.

Twinfilin controls the dynamics of CP in cells

Twinfilin binds CP through its C-terminal tail[41,42,66], and both twinfilin and CP localize to lamellipodia in mammalian cells[14,43,67,68]. Whereas CP localizes to the distal edge of lamellipodia[14], the precise localization of twinfilin has not been reported. We thus expressed EGFP-CP and EGFP-twinfilin-1 in B16-F1 cells and compared their localizations to AlexaFluor-568-phalloidin labelled actin filaments in maximum intensity projection images generated from confocal microscope stacks. Line profile analysis revealed that, whereas CP was enriched at the distal edge of lamellipodial F-actin network, twinfilin localized throughout the lamellipodium (Figure 4a-d). FRAP experiments revealed that EGFP-twinfilin-1 does not display retrograde movement with the lamellipodial actin filament network, but instead recovers progressively across the whole lamellipodial network, being a dynamic component of the lamellipodium ($t_{1/2}$ ~1.5 s, Figure 4 e-f, Supplementary video 5).

We next examined if twinfilin regulates CP in cells. Expression level of CP was not altered upon depletion of twinfilin (Extended Data Fig. 2b). However, in the absence of twinfilins, CP was no longer

restricted to the leading edge of lamellipodium, but its localization spread throughout the lamellipodial actin filament network (Figure 4g-j). Importantly, FRAP experiments revealed that also the dynamics of CP was drastically altered in twinfilin-deficient cells. Instead of dynamic exchange at the distal edge of lamellipodium observed in wild-type cells[37], CP displayed stable association with the actin filament network and displayed movement along the retrograde actin flow in lamellipodia of twf1/twf2-KO cells (Figure 5a-b, Supplementary videos 6-7). We note that in twf1/twf2-KO cells EGFP-CP exhibits a two-phase recovery, from which the fast recovery phase most likely corresponds to soluble EGFP-CP.

Because both twinfilin and CP localize to endocytic actin filament structures[47,69], we examined CP dynamics also in these structures. Wild-type and twf1/twf2-KO cells were co-transfected with plasmids expressing Cherry-LifeAct to mark actin structures, and EGFP-CP for FRAP analysis (Figure 5c-d, Supplementary video 8). These experiments revealed that EGFP-CP displayed ~10-fold decreased recovery rate at the endosomal actin structures of twf1/twf2-KO cells compared to the wild-type cells (Figure 5e). Thus, twinfilin is critical for rapid CP dynamics in lamellipodial and endocytic actin filament structures.

Twinfilin uncaps filament barbed ends *in vitro*

To test if twinfilin regulates CP dynamics directly by uncapping filament barbed ends, we performed experiments on single filaments inside a microfluidics chamber with purified mouse twinfilin and chicken CP[35]. Actin filaments were polymerized from spectrin-actin seeds bound non-specifically on the glass surface, and were subsequently capped by CP (Figure 6a). In the absence of twinfilin, filament length was very stable indicating that filaments were capped at their barbed ends. In the presence of twinfilin-1, a large fraction of filaments began to depolymerize, indicating that they were uncapped (Figure 6b). By performing the assay with different twinfilin concentrations, we estimated a Kd of ~300 nM for twinfilin to CP-capped actin filament barbed ends and revealed that, at saturating

conditions, twinfilin accelerated filament uncapping by ~6-fold. Filament uncapping was further enhanced by including CP-sequestering protein V-1 to the reactions. Whereas V-1 alone does not accelerate CP dissociation, twinfilin and V-1 together increased the uncapping rate by ~40-fold compared to the buffer control (Figure 6c). Earlier studies with animal cells revealed that stabilization of lamellipodial actin networks with jasplakinolide prolonged CP lifetime in lamellipodia[38]. Our *in vitro* uncapping experiments in the presence of G-actin revealed that phalloidin-stabilization had no impact on the uncapping activity of twinfilin (Extended Data Fig. 5a).

Both CARMIL1 and ADF/cofilin enhance CP dissociation from filament barbed ends *in vitro*[35,39]. Similar to the study by Johnston et al.[43], our experiments demonstrated that full-length twinfilin and the CARMIL homology 3 (CAH3) domain of CARMIL1 compete in binding to CP. CAH3 accelerated CP dissociation more efficiently compared to twinfilin-1. Due to competitive binding, twinfilin-1 added to CAH3 reduced the observed uncapping rate, which became closer to that in the presence of twinfilin alone, but remained far above the spontaneous uncapping rate in the absence of twinfilin and CAH3 (Extended Data Fig. 5b).

In cells, CARMIL1 localization to lamellipodia was not affected by depletion of twinfilin (Extended Data Fig. 6a-b). As reported earlier[29,70], depletion of CARMIL1 resulted in a different phenotype compared to the one of twf1/twf2 knockout cells, characterized by defective lamellipodia formation and loss of CP at the cell edge (Extended Data Fig. 6c). Over-expression of mCherry-CARMIL1 in twf1/twf2-KO cells moderately enhanced the dynamics of CP, but CP still displayed abnormal localization across the lamellipodium (Extended Data Fig. 6d, Supplementary video 9). We also revealed that over-expression of the major ADF/cofilin isoform, cofilin-1, did not increase CP dynamics in the lamellipodia of twf1/twf2-knockout cells (Extended Data Fig. 7a-c, Supplementary video 10). We note that EGFP-CP fluorescence did not reach complete recovery during the 40 s observation period due to slow dynamics of CP in the absence of twinfilins.

These experiments reveal that twinfilin uncaps actin filaments *in vitro*. Although both CARMIL and ADF/cofilins can accelerate CP dynamics *in vitro,* they cannot rescue the abnormal CP dynamics in twinfilin-depleted cells, demonstrating that the filament uncapping function reported here is specific to twinfilin.

Actin-binding activity of twinfilin is required for filament uncapping

To uncover if twinfilin uncaps filament barbed ends through interacting with CP, actin filament barbed ends, or both, we purified mutant twinfilins that displayed defects in either binding to CP (F323A,K325A,K327A = tail mutant)[42] or actin (R96A,K98A,R267A,R269A = ADF-H domain mutant)[48,65] (Figure 7a). The mutant defective in interacting with CP uncapped actin filaments *in vitro* even more efficiently compared to wild-type twinfilin. In contrast, the ADF-H domain mutant did not exhibit detectable uncapping activity, demonstrating that twinfilin's ability to bind actin filament barbed ends is critical for dissociation of CP from filament ends (Figure 7b).

We next expressed mCherry-fusions of wild-type and mutant twinfilin-1 in twf1/twf2-KO cells, and studied by FRAP if they can rescue the diminished EGFP-CP dynamics (Figure 7c, Supplementary videos 11-13). Expression of mCherry-tagged wild-type twinfilin-1 rescued CP dynamics back to levels of wild-type B16-F1 cells (Figure 7d, supplementary video 11). Consistent with the *in vitro* experiments, the ADF-H domain mutant did not rescue the slow CP dynamics, whereas the tail mutant rescued the phenotype nearly as well as the wild-type mCherry-twinfilin-1 (Figure 7d, Supplementary video 12-13). Please note that EGFP-tagged twinfilin-1 tail mutant appears to display more diffuse sub-cellular localization compared to the wild-type protein (Figure 8a-d). Thus, defective localization of the twinfilin tail mutant to lamellipodial actin networks provides a plausible explanation for the discrepancy between our *in vitro* single filament uncapping and cellular data on this mutant.

Collectively, these results demonstrate that twinfilin's ability to bind actin through its two ADF-H domains is critical for filament uncapping.

DISCUSSION

Regulation of CP in cells is orchestrated by a large number of proteins[9,10,24]. To date, the CPI-motif containing proteins, such as CARMILs, were considered as the best candidates to uncap filament barbed ends, because *in vitro* CARMILs decrease the affinity of CP towards barbed ends through allosteric competition[25,26,28,39]. However, to our knowledge, there is no direct cell biological evidence to support the role of CARMIL as an uncapping factor. Moreover, CP fails to localize to lamellipodia in CARMIL-depleted cells[29]. Thus, it is more plausible that CARMIL functions as a 'pro-capping' protein, which retrieves CP from CP/V-1 complex and allows it to associate with filament barbed ends close to the plasma membrane[9,22,24]. Our cell biological and biochemical work provide strong evidence that twinfilin is a critical factor that is responsible for rapid dynamics and specific subcellular localization of CP in cells. Moreover, single filament experiments provide evidence that twinfilin sequesters actin monomers, inhibits filament barbed end elongation, and allows actin filaments to depolymerize following dissociation of CP.

We revealed that actin-binding, but not its interaction with CP, is critical for the actin filament uncapping by twinfilin both *in vitro* and in cells. Thus, rather than binding to CP through the CPI motif, twinfilin competes directly with CP for filament barbed end binding, and subsequently dissociates CP (Figure 8e). Interestingly, the twinfilin mutant unable to interact with CP displayed elevated uncapping activity compared to the wild-type protein. We hypothesize that the CPI motif of twinfilin can still interact with CP when twinfilin is bound to filament barbed ends, thus serving as a transition complex for uncapped/capped barbed ends. This is supported by the fact that the CP-sequestering protein, V-1,

enhances uncapping by twinfilin. We hypothesize that V-1 is able to bind CP in the presence of twinfilin after CP dissociates from the filament barbed end. We also note that ADF/cofilins, which are composed of a single ADF-H domain that is structurally similar to the two ADF-H domains of twinfilin[71,72], dissociate CP if the ADF/cofilin-decorated segment reaches the filament barbed end[35]. Thus, we speculate that one of the twinfilin ADF-H domains may first bind to the side of the filament and change the conformation of terminal actin subunits, thus weakening the affinity of CP to the barbed ends. Subsequently, the other ADF-H domain of twinfilin would associate with the terminal actin subunit to displace CP.

An earlier study suggested that twinfilin may function as a 'pro-capping' factor by loading CP to filament barbed ends by interacting with CP[43]. Our biochemical experiments are consistent with these observations (Extended Data Fig. 5b), but our cell biological data are contradictory with the capping protein activation model proposed for twinfilin[43]. This is because EGFP-CP was efficiently recruited to lamellipodial actin filaments also in the absence of twinfilin, and because inhibition of twinfilin-CP interaction through specific point mutations did not drastically affect CP localization in cells. Thus, twinfilin-CP interaction is not necessary for CP-activation in lamellipodia, suggesting that other CPI motif-containing proteins, such as CARMILs, are the primary activators of CP. Interaction with CP enhances the localization of twinfilin to endocytic actin patches in budding yeast[41,66], and mutations in the CPI-motif of mouse twinfilin-1 appear to affect its localization to lamellipodia in B16-F1 cells (Figure 8a-d). Thus, CPI motif in twinfilin may serve as a targeting signal that directs twinfilin to CP-rich actin filaments, and hence enhances filament uncapping activity of twinfilin in cells.

A working model for how twinfilin regulates the dynamics of lamellipodial actin networks is presented in Figure 8f-g. Twinfilin restricts localization of CP to the distal edge of lamellipodium by uncapping filament barbed ends as filaments display retrograde flow away from the membrane. The trigger for twinfilin to uncap filament barbed ends remains enigmatic, but may be related to ATP-hydrolysis in

actin. Twinfilin binds ADP-F-actin barbed ends with higher affinity than ATP-F-actin barbed ends[47], and may uncap filament barbed ends only after nucleotide hydrolysis and Pi-release occurred in the terminal actin subunits. Our experiments and a recent study[73] revealed that at high concentration twinfilin allows actin filament depolymerization also under assembly-promoting conditions suggesting that in cells the filaments uncapped by twinfilin may still undergo barbed end depolymerization with a rate of ~6 subunits/s. Thus, twinfilin is able to inhibit actin polymerization after dissociation of CP through sequestering actin monomers and by interacting with filament barbed ends. It is important to note that ADF/cofilin and cyclase-associated-protein can synergistically promote filament pointed end depolymerization with a rate up to ~20 subunit/s[74,75]. Therefore, in wild-type cells depolymerization of 'aged' actin filaments from both barbed and pointed ends may have an important role in actin turnover, as proposed by Wioland et. al.[35]. In the absence of twinfilin, CP remains stably bound to filament barbed ends throughout the lamellipodia, and thus actin dynamics relies entirely on filament depolymerization from their pointed ends. This model also provides a plausible explanation for diminished actin filament turnover rates in twf1/twf2-KO cells, although the precise contribution of filament barbed end depolymerization in turnover dendritic actin networks remains to be shown.

Besides twinfilin and V-1, other factors contribute to rapid CP dynamics in cells. This is because *in vitro*, the combined action of twinfilin and V-1 accelerates the uncapping rate to 0.0067 s^{-1} that is still much slower than the off-rate of CP in cells (approximately 0.3 s^{-1}). ADF/cofilin is a likely candidate to regulate CP dynamics, as it promotes filament severing and debranching, and as it reduces the affinity of CP for the barbed ends of filaments that are reached by ADF/cofilin domains[35]. Our experiments on cells, however, provided evidence that ADF/cofilin and twinfilin accelerate actin filament uncapping through non-overlapping mechanisms. Importantly, also ADF/cofilin-catalyzed filament severing and debranching contribute to rapid CP dynamics in lamellipodia[38]. Our efforts to assess the combined effect of twinfilin and ADF/cofilin *in vitro* on single filaments were unsuccessful due to excessive filament

sticking to the surface in the presence of both proteins. Thus, future studies are needed to uncover the possible synergies between direct filament uncapping by twinfilin and the multiple actions of ADF/cofilin, as well as the contribution of ADF/cofilin cofactors and filament debranching by GMF[76,77] in rapid CP dynamics.

In addition to lamellipodial actin dynamics, twinfilin has been linked to endocytosis[51,78], lymphoma progression[79], chemotherapy resistance[53], cardiac hypertrophy[80], cancer cell invasion[81], platelet reactivity and turnover[52], and regulation of cochlear stereocilia length[82]. In the future, it will be important to examine if twinfilin contributes also to these processes by uncapping filament barbed ends, and subsequently allowing filament depolymerization. Additionally, whether the muscle specific twinfilin isoform, twinfilin-2b[54], functions as a regulator of CP dynamics in muscle cells remains to be studied.

ACKNOWLEDGEMENTS

We thank Ville Paavilainen, and Juha Saarikangas for critical reading of the manuscript. Institute of Biotechnology Light Microscopy Unit, Biomedicum Imaging Unit and Institute of Molecular Medicine Finland High Content Imaging and Analysis Unit are acknowledged for providing support in imaging and image analysis. We thank Mirva Tirkkonen for technical assistance. This study was supported by grants from Academy of Finland (302161) and Cancer Society Finland (4705949) to P.L., from Doctoral School in Health Sciences at University of Helsinki to M.H and T.K., and from the Agence Nationale de la Recherche (Grant Muscactin) to G.R-L. and from the European Research Council (Grant StG-679116) to A.J.

AUTHOR CONTRIBUTIONS

P.L. and M.H. crafted the original idea, and M.H., H.W., A.J., G.R-L., and P.L. designed the experiments. M.H., M.T., T.K., A.J., and H.W. performed the experiments, and M.H., A.J., and H.W. analyzed the data. M.H. and P.L. drafted the manuscript with contribution from all authors. P.L., A.J., and G.R-L. acquired the funding.

COMPETING INTERESTS

The authors declare no competing interests.

REFERENCES

1. Kaksonen, M., Toret, C. & Drubin, D. Harnessing actin dynamics for clathrin-mediated endocytosis. *Nat. Rev. Mol. Cell Biol.* **7**, 404–14 (2006).

2. Svitkina, T. Ultrastructure of the actin cytoskeleton. *Curr. Opin. Cell Biol.* **54**, 1–8 (2018).

3. Senju, Y. & Lappalainen, P. Regulation of actin dynamics by PI(4,5)P2 in cell migration and endocytosis. *Curr. Opin. Cell Biol.* **56**, 7–13 (2019).

4. Rottner, K. & Schaks, M. Assembling actin filaments for protrusion. *Curr. Opin. Cell Biol.* **56**, 53–63 (2019).

5. De Melo, L. *et al.* Evolutionary conservation of actin-binding proteins in Trypanosoma cruzi and unusual subcellular localization of the actin homologue. *Parasitology* **135**, 955–965 (2008).

6. Pollard, T. D. & Borisy, G. G. Cellular motility driven by assembly and disassembly of actin filaments. *Cell* **112**, 453–465 (2003).

7. Cooper, J. & Schafer, D. Control of actin assembly and disassembly at filament ends. *Curr. Opin. Cell Biol.* **12**, 97–103 (2000).

8. Carlier, M.-F. & Pantaloni, D. Control of actin dynamics in cell motility. *J. Mol. Biol.* **269**, 459–67 (1997).

9. Edwards, M. *et al.* Capping protein regulators fine-tune actin assembly dynamics. *Nature Reviews Molecular Cell Biology* **15**, 677–689 (2014).

10. Shekhar, S., Pernier, J. & Carlier, M.-F. Regulators of actin filament barbed ends at a glance. *J. Cell Sci.* **129**, 1085–1091 (2016).

11. Loisel, T., Boujemaa, R., Pantaloni, D. & Carlier, M.-F. Reconstitution of actin-based motility of Listeria and Shigella using pure proteins. *Nature* **401**, 613–616 (1999).

12. Amatruda, J., Cannon, J., Tatchell, K., Hug, C. & Cooper, J. Disruption of the actin cytoskeleton in yeast capping protein mutants. *Nature* **344**, 352–354 (1990).

13. Amatruda, J., Gattermeir, D., Karpova, T. & Cooper, J. Effects of null mutations and overexpression of capping protein on morphogenesis, actin distribution and polarized secretion in yeast. *J. Cell Biol.* **119**, 1151–1162 (1992).

14. Mejillano, M. *et al.* Lamellipodial versus filopodial mode of the actin nanomachinery. *Cell* **118**, 363–373 (2004).

15. Iwasa, J. & Mullins, R. D. Spatial and temporal relationships between actin-filament nucleation, capping, and disassembly. *Curr. Biol.* **17**, 395–406 (2007).

16. Rogers, S., Wiedemann, U., Stuurman, N. & Vale, R. Molecular requirements for actin-based lamella formation in Drosophila S2 cells. *J. Cell Biol.* **162**, 1079–1088 (2003).

17. Kim, K., Yamashita, A., Wear, M., Maéda, Y. & Cooper, J. Capping protein binding to actin in yeast: biochemical mechanism and physiological relevance. *J. Cell Biol.* **164**, 567–80 (2004).

18. Sinnar, S., Antoku, S., Saffin, J.-M., Cooper, J. & Halpain, S. Capping protein is essential for cell migration in vivo and for filopodial morphology and dynamics. *Mol. Biol. Cell* **25**, 2152–2160 (2014).

19. Akin, O. & Mullins, R. D. Capping protein increases the rate of actin-based motility by promoting filament nucleation by the Arp2/3 complex. *Cell* **133**, 841–851 (2008).

20. Bhattacharya, N., Ghosh, S., Sept, D. & Cooper, J. Binding of myotrophin/V-1 to actin-capping protein: Implications for how capping protein binds to the filament barbed end. *J. Biol. Chem.* **281**, 31021–31030 (2006).

21. Jung, G. *et al.* V-1 regulates Capping Protein activity in vivo. *Proc. Natl. Acad. Sci. U. S. A.* **113**, E6610–E6619 (2016).

22. Fujiwara, I., Remmert, K., Piszczek, G. & Hammer, J. Capping protein regulatory cycle driven by CARMIL and V-1 may promote actin network assembly at protruding edges. *Proc. Natl. Acad. Sci. U. S. A.* **111**, E1970-9 (2014).

23. Taoka, M. *et al.* V-1, a protein expressed transiently during murine cerebellar development, regulates actin polymerization via interaction with capping protein. *J. Biol. Chem.* **278**, 5864–70 (2003).

24. Stark, B., Lanier, M. H. & Cooper, J. CARMIL family proteins as multidomain regulators of actin-based motility. *Mol. Biol. Cell* **28**, 1713–1723 (2017).

25. Takeda, S. *et al.* Two distinct mechanisms for actin capping protein regulation-steric and

allosteric inhibition. *PLoS Biol.* **8**, e1000416 (2010).

26. Uruno, T., Remmert, K. & Hammer, J. CARMIL is a potent capping protein antagonist: Identification of a conserved CARMIL domain that inhibits the activity of capping protein and uncaps capped actin filaments. *J. Biol. Chem.* **281**, 10635–10650 (2006).

27. Yang, C. *et al.* Mammalian CARMIL inhibits actin filament capping by capping protein. *Dev. Cell* **9**, 209–221 (2005).

28. Hernandez-Valladares, M. *et al.* Structural characterization of a capping protein interaction motif defines a family of actin filament regulators. *Nat. Struct. Mol. Biol.* **17**, 497–503 (2010).

29. Edwards, M., Liang, Y., Kim, T. & Cooper, J. A. Physiological role of the interaction between CARMIL1 and capping protein. *Mol. Biol. Cell* **24**, 3047–3055 (2013).

30. Edwards, M., McConnell, P., Schafer, D. & Cooper, J. CPI motif interaction is necessary for capping protein function in cells. *Nat. Commun.* **6**, 8415 (2015).

31. Park, L. *et al.* Cyclical Action of the WASH Complex: FAM21 and Capping Protein Drive WASH Recycling, Not Initial Recruitment. *Dev. Cell* **24**, 169–181 (2013).

32. Zhao, J. *et al.* CD2AP Links Cortactin and Capping Protein at the Cell Periphery To Facilitate Formation of Lamellipodia. *Mol. Cell. Biol.* **33**, 38–47 (2013).

33. Lanier, M. H., McConnell, P. & Cooper, J. Cell migration and invadopodia formation require a membrane-binding domain of CARMIL2. *J. Biol. Chem.* **291**, 1076–1091 (2016).

34. Schafer, D., Jennings, P. & Cooper, J. Dynamics of capping protein and actin assembly in vitro: uncapping barbed ends by polyphosphoinositides. *J. Cell Biol.* **135**, 169–79 (1996).

35. Wioland, H. *et al.* ADF/cofilin accelerates actin dynamics by severing filaments and promoting their depolymerization at both ends. *Curr. Biol.* **27**, 1956-1967.e7 (2017).

36. Kim, T., Cooper, J. & Sept, D. The interaction of capping protein with the barbed end of the actin filament. *J. Mol. Biol.* **404**, 794–802 (2010).

37. Lai, F. *et al.* Arp2/3 complex interactions and actin network turnover in lamellipodia. *EMBO J.* **27**, 982–92 (2008).

38. Miyoshi, T. *et al.* Actin turnover-dependent fast dissociation of capping protein in the dendritic nucleation actin network: Evidence of frequent filament severing. *J. Cell Biol.* **175**, 947–955 (2006).

39. Fujiwara, I., Remmert, K. & Hammer, J. Direct observation of the uncapping of capping protein-capped actin filaments by CARMIL homology domain 3. *J. Biol. Chem.* **285**, 2707–2720 (2010).

40. Poukkula, M., Kremneva, E., Serlachius, M. & Lappalainen, P. Actin-depolymerizing factor homology domain: a conserved fold performing diverse roles in cytoskeletal dynamics. *Cytoskeleton* **68**, 471–490 (2011).

41. Falck, S. *et al.* Biological role and structural mechanism of twinfilin-capping protein interaction. *EMBO J.* **23**, 3010–3019 (2004).

42. Hakala, M., Kalimeri, M., Enkavi, G., Vattulainen, I. & Lappalainen, P. Molecular mechanism for inhibition of twinfilin by phosphoinositides. *J. Biol. Chem.* **293**, 4818–4829 (2018).

43. Johnston, A. *et al.* A novel mode of Capping Protein-regulation by twinfilin. *Elife* **7**, e41313 (2018).

44. Goode, B., Drubin, D. & Lappalainen, P. Regulation of the cortical actin cytoskeleton in

budding yeast by twinfilin, a ubiquitous actin monomer-sequestering protein. *J. Cell Biol.* **142**, 723–733 (1998).

45. Vartiainen, M., Ojala, P., Auvinen, P., Peränen, J. & Lappalainen, P. Mouse A6/twinfilin is an actin monomer-binding protein that localizes to the regions of rapid actin dynamics. *Mol. Cell Biol.* **20**, 1772–1783 (2000).

46. Ojala, P. *et al.* The two ADF-H domains of twinfilin play functionally distinct roles in interactions with actin monomers. *Mol. Biol. Cell* **13**, 3811–3821 (2002).

47. Helfer, E. *et al.* Mammalian twinfilin sequesters ADP-G-actin and caps filament barbed ends: implications in motility. *EMBO J.* **25**, 1184–1195 (2006).

48. Johnston, A., Collins, A. & Goode, B. High-speed depolymerization at actin filament ends jointly catalysed by twinfilin and Srv2/CAP. *Nat. Cell Biol.* **17**, 1504–1511 (2015).

49. Hilton, D., Aguilar, R., Johnston, A. & Goode, B. Species-specific functions of twinfilin in actin filament depolymerization. *J. Mol. Biol.* **430**, 3323–3336 (2018).

50. Wahlström, G. *et al.* Twinfilin is required for actin-dependent developmental processes in Drosophila. *J. Cell Biol.* **155**, 787–796 (2001).

51. Wang, D. *et al.* Drosophila twinfilin is required for cell migration and synaptic endocytosis. *J. Cell Sci.* **123**, 1546–1556 (2010).

52. Stritt, S. *et al.* Twinfilin 2a is a regulator of platelet reactivity and turnover in mice. *Blood* **130**, 1746–1756 (2017).

53. Bockhorn, J. *et al.* MicroRNA-30c inhibits human breast tumour chemotherapy resistance by regulating TWF1 and IL-11. *Nat. Comm.* **4**, e1393 (2013).

54. Nevalainen, E., Skwarek-Maruszewska, A., Braun, A., Moser, M. & Lappalainen, P. Two biochemically distinct and tissue-specific twinfilin isoforms are generated from the mouse Twf2 gene by alternative promoter usage. *Biochem. J* **417**, 593–600 (2009).

55. Abella, J. V. G. *et al.* Isoform diversity in the Arp2/3 complex determines actin filament dynamics. *Nat. Cell Biol.* **18**, 76–86 (2016).

56. Kapustina, M., Read, T. A. & Vitriol, E. A. Simultaneous quantification of actin monomer and filament dynamics with modeling-assisted analysis of photoactivation. *J. Cell Sci.* **129**, 4633–4643 (2016).

57. Burnette, D. T. *et al.* A role for actin arcs in the leading-edge advance of migrating cells. *Nat. Cell Biol.* **13**, 371–81 (2011).

58. Carlier, M. F., Romet-Lemonne, G. & Jégou, A. Actin filament dynamics using microfluidics. *Methods Enzymol.* **540**, 3–17 (2014).

59. Jégou, A., Carlier, M. F. & Romet-Lemonne, G. Microfluidics pushes forward microscopy analysis of actin dynamics. *Bioarchitecture* **1**, 271–276 (2011).

60. Pollard, T. Rate constants for the reactions of ATP- and ADP-actin with the ends of actin filaments. *J. Cell Biol.* **103**, 2747–2754 (1986).

61. Carlier, M. F., Criquet, P., Pantaloni, D. & Korn, E. D. Interaction of cytochalasin D with actin filaments in the presence of ADP and ATP. *J. Biol. Chem.* **261**, 2041–2050 (1986).

62. Fujiwara, I., Zweifel, M. E., Courtemanche, N. & Pollard, T. D. Latrunculin A Accelerates Actin Filament Depolymerization in Addition to Sequestering Actin Monomers. *Curr. Biol.* **28**, 3183-3192.e2 (2018).

63. Coue, M. & Korn, E. D. Interaction of plasma gelsolin with G-actin and F-actin in the presence and absence of calcium ions. *J. Biol. Chem.* **260**, 15033–15041 (1985).

64. Kuhn, J. R. & Pollard, T. D. Real-time measurements of actin filament polymerization by total internal reflection fluorescence microscopy. *Biophys. J.* **88**, 1387–1402 (2005).

65. Paavilainen, V. *et al.* Structural basis and evolutionary origin of actin filament capping by twinfilin. *Proc. Natl. Acad. Sci.* **104**, 3113–3118 (2007).

66. Palmgren, S., Ojala, P., Wear, M., Cooper, J. & Lappalainen, P. Interactions with PIP2, ADP-actin monomers, and capping protein regulate the activity and localization of yeast twinfilin. *J. Cell Biol.* **155**, 251–260 (2001).

67. Vartiainen, M., Sarkkinen, E., Matilainen, T., Salminen, M. & Lappalainen, P. Mammals have two twinfilin isoforms whose subcellular localizations and tissue distributions are differentially regulated. *J. Biol. Chem.* **278**, 34347–34355 (2003).

68. Schafer, D. *et al.* Visualization and molecular analysis of actin assembly in living cells. *J. Cell Biol.* **143**, 1919–1930 (1998).

69. Kaksonen, M., Toret, C. P. & Drubin, D. G. A modular design for the clathrin- and actin-mediated endocytosis machinery. *Cell* **123**, 305–320 (2005).

70. Liang, Y., Niederstrasser, H., Edwards, M., Jackson, C. E. & Cooper, J. A. Distinct roles for CARMIL isoforms in cell migration. *Mol. Biol. Cell* **20**, 5290–5305 (2009).

71. Paavilainen, V. *et al.* Structural conservation between the actin monomer-binding sites of twinfilin and actin-depolymerizing factor (ADF)/cofilin. *J. Biol. Chem.* **277**, 43089–43095 (2002).

72. Paavilainen, V., Oksanen, E., Goldman, A. & Lappalainen, P. Structure of the actin-depolymerizing factor homology domain in complex with actin. *J. Cell Biol.* **182**, 51–59 (2008).

73. Shekhar, S., Hoeprich, G. J., Gelles, J. & Goode, B. L. Twinfilin bypasses assembly conditions and actin filament aging to drive barbed end depolymerization. *J. Cell Biol.* **220**, e202006022 (2020).

74. Kotila, T. *et al.* Mechanism of synergistic actin filament pointed end depolymerization by cyclase-associated protein and cofilin. *Nat. Commun.* **10**, 5320 (2019).

75. Shekhar, S., Chung, J., Kondev, J., Gelles, J. & Goode, B. Synergy between Cyclase-associated protein and Cofilin accelerates actin filament depolymerization by two orders of magnitude. *Nat. Commun.* **10**, 5319 (2019).

76. Poukkula, M. *et al.* GMF promotes leading-edge dynamics and collective cell migration in vivo. *Curr. Biol.* **24**, 2533–40 (2014).

77. Haynes, E. M. *et al.* GMFβ controls branched actin content and lamellipodial retraction in fibroblasts. *J. Cell Biol.* **209**, 803–812 (2015).

78. Pelkmans, L. *et al.* Genome-wide analysis of human kinases in clathrin- and caveolae/raft-mediated endocytosis . *Nature* **436**, 78–86 (2005).

79. Meacham, C., Ho, E., Dubrovsky, E., Gertler, F. & Hemann, M. In vivo RNAi screening identifies regulators of actin dynamics as key determinants of lymphoma progression. *Nat. Genet.* **41**, 1133–1137 (2009).

80. Li, Q. *et al.* Attenuation of microRNA-1 derepresses the cytoskeleton regulatory protein twinfilin-1 to provoke cardiac hypertrophy. *J. Cell Sci.* **123**, 2680–2680 (2010).

81. Bockhorn, J. *et al.* MicroRNA-30c targets cytoskeleton genes involved in breast cancer cell invasion. *Breast Cancer Res. Treat.* **137**, 373–82 (2013).

82. Peng, A., Belyantseva, I., Hsu, P., Friedman, T. & Heller, S. Twinfilin-2 regulates actin filament lengths in cochlear stereocilia. *J. Neurosci.* **29**, 15083–15088 (2009).

FIGURE LEGENDS

Figure 1. Knockout of twinfilins leads to F-actin accumulation in the lamellipodia and perinuclear region. a. Representative examples of maximum intensity projection images of confocal stacks of wild-type and twinfilin knockout mouse B16-F1 cells stained with AlexaFluor-568 phalloidin and anti-p34 antibody, respectively. Scale bar = 10 μm. Experiment was repeated three times. **b**. Normalized F-actin intensity in wild-type and twinfilin knockout B16-F1 cells. The median, 25th and 75th percentiles and the minimum and maximum values of the data are shown. Number of analyzed cells were: B16-F1 wt = 1,958, twf1-KO-g1 = 1,045, twf2-KO-g3#1 = 1,285, twf1/2-KO-g3 = 1,265, twf1/2-KO-g4 = 1,707 from two experiments. **c.** A representative maximum intensity projection image of confocal stacks image of twf1/twf2-KO cells transiently expressing EGFP-TWF1 and stained with AlexaFluor-568 phalloidin. Scale bar = 10 μm. Image is representative of three experiments. **d.** F-actin intensities in the cytoplasmic regions of wild-type, twf1/twf2-KO, and knockout cells expressing EGFP-TWF-1. The median, 25th and 75th percentiles and the minimum and maximum values of the data are shown. Number of cells analyzed were: B16-F1 wt = 4,875, twf1/twf2-KO-g3 = 5,731, twf1/twf2-KO-g3 + EGFP-TWF-1 = 197 from three experiments. **e.** F-actin intensities in the lamellipodial regions. **f.** The Arp2/3 complex intensities in the lamellipodial regions. Number of cells analyzed in panels e and f were B16-F1 wt = 49, twf1/twf2-KO g3 = 50, twf1/twf2-KO g3 + EGFP-TWF-1 = 49, from three experiments. **g.** Representative kymographs and quantification of lamellipodia

protrusion velocities of wild-type (n = 18), twf1/twf-2 knockout (n = 14), and knockout cells expressing EGFP-TWF-1 (n = 22) from three experiments. **h.** Cell migration speeds of wild-type (n = 29) and twf1/twf2 g3 (n = 38) and twf1/twf2 g4 (n = 44) knockout cells from three replicate random cell migration assays. Data in (e-h) represent individual cells with mean and standard deviations shown. Statistical source data are provided in Source Data Fig. 1.

Figure 2. Twinfilin regulates actin dynamics in lamellipodia. a. Representative examples of fluorescence recovery after photobleaching (FRAP) of EGFP-actin in wild-type and twf1/twf2-KO B16-F1 cells. Timepoint "Pre" is a frame before bleaching, and 0 s is the first frame after bleaching. Scale bar = 5 μm. **b-c.** Examples of kymographs created from the center of the bleached region in lamellipodia of wild-type (panel b) and twf1/twf2-KO B16-F1 cells (panel c). F-actin network assembly rates were measured as a sum of protrusion velocity and retrograde flow. **d.** F-actin network assembly rates in the lamellipodia of wild-type and twf1/twf2-KO B16-F1 cells. Data represent individual measurements (n = 15) from three experiments, and the mean values are indicated by horizontal lines. **e.** Representative examples of photoactivation of PA-GFP-β-actin in wild-type and twf1/twf2-KO B16-F1 cells co-expressing mCherry-LifeAct as marker for lamellipodia, and knockout-rescue cells co-expressing mCherry-TWF-1. Timepoint "Pre" is a frame before photoactivation and 0 s is the first frame after the activation. Scale bar = 5 μm. **f.** Analysis of the PA-GFP-actin fluorescence decay. Data represent mean of n=11 (B16-F1 wild type), n=8 (twf1/twf2-KO cells) and n=16 (twf1/twf2-KO + mCherry-TWF1 rescue) measurements from three experiments with shaded surfaces representing standard deviations. Halftimes for GFP-actin fluorescence decays: B16-F1 = 13.1 s, twf-1/2-KO = 22.5 s, twf-1/2-KO + mCherry-TWF-1 rescue = 14.6 s. Statistical source data are provided in Source Data Fig. 2.

Figure 3. Twinfilin does not accelerate barbed end depolymerization. a. Rationale of the depolymeirzation experiment using microfluidics (left), and representative examples of individual filaments during depolymerization experiments performed in the absence and presence of 1 μM TWF-1 (right). Scale bar = 5 μm. **b.** Barbed end depolymerization of ADP-actin filaments in presence of different concentrations of TWF-1. Data points represent median values of n=20 filaments from one experiment with 25^{th} and 75^{th} percentiles shown. **c.** Barbed end depolymerization of ADP-actin filaments in the presence of TWF-1 and/or N-CAP1. Data points represent individual measurements (n = 20 for TWF-1 alone, N-CAP1 alone, and TWF-1+N-CAP1 from one experiment, and n=40 for buffer control from two experiments), with mean and standard deviations shown. **d.** Polymerization of actin filaments at barbed ends in presence of 4 μM ATP-G-actin and 4 μM profilin, and different concentrations of TWF-1. Scale bar = 5 μm. **e.** Analysis of actin filament barbed end polymerization in the presence of 0.4 μM ATP-G-actin (orange), 2 μM ATP-G-actin and 2 μM profilin (blue), or 4 μM ATP-G-actin and 4 μM profilin (purple), and different concentrations of TWF-1. Positive and negative values on y-axis indicate filament polymerization and depolymerization, respectively. Data points represent median values with 25^{th} and 75^{th} percentiles shown. Number of measured filaments (n) from independent experiments (N) were for 0.4 μM G-actin: 0 μM TWF-1 (n=61, N=3), 0.067 μM and 0.268 μM TWF-1 (n=20, N=1), 0.5 μM TWF-1 (n=61, N=3), 1 μM and 2.7 μM TWF-1 (n=20, N=2), and 2 μM TWF-1 (n=21, N=2); for 2 μM G-actin + 2 μM profilin: 0 μM TWF-1 (n=40, N=2), 0.5-5 μM TWF-1 (n=20, N=1); and for 4 μM G-actin + 4 μM profilin: 0 μM and 0.5 μM TWF-1 (n=60, N=3), 0.25 μM TWF-1 (n=42, N=2), 1 and 2 μM TWF-1 (n=20, N=1), 4 μM TWF-1 (n=24, N=1), 6 μM TWF-1 (n=39, N=2), and 8 μM TWF-1 (n=21, N=1). Statistical source data are provided in Source Data Fig. 3.

Figure 4. Twinfilin and capping protein display different localizations and dynamics in lamellipodia. Representative examples of EGFP-TWF-1 (**a**) and EGFP-CP (**b**) localizations in the lamellipodia of mouse B16-F1 cells from experiments in panels c-d. Scale bars in panels **a.** and **b.** = 10 μm. Images in the middle and right in panels **a-b.** are magnifications of lamellipodial regions highlighted in the images on the left. F-actin was visualized by AlexaFluor-568 phalloidin. **c-d.** Line profiles were generated across the center of lamellipodia as indicated with dotted lines. Data represent mean of n=22 (panel **c**) and n=24 (panel **d**) cells from one experiment, with standard deviations shown. The '0 μm' value in the x-axis is set to correspond to the peak intensity of phalloidin. **e.** Fluorescence recovery after photobleaching of EGFP-TWF-1 in a mouse B16-F1 cell lamellipodium. Time-point "Pre" is a frame before bleaching with a bleached region indicated with dotted square, and 0 s the first frame after the bleaching. Scale bar = 5 μm. **f.** Analysis of EGFP-TWF-1 fluorescence recovery. Data represent mean of n=8 measurements from two experiments with shaded surfaces representing standard deviations. Recovery halftime for EGFP-TWF-1 was ~ 1.5 s. **g.** Representative images of EGFP-CP localization in wild-type and twf1/twf2-KO B16-F1 cells, where F-actin was visualized with AlexaFluor-568 phalloidin. Panels in the middle and right are magnifications of lamellipodial regions highlighted in the whole cell images on the left. Scale bars = 10 μm. **h-i.** Examples of line profiles generated across the center of lamellipodia as indicated with dotted lines in B16-F1 wild type (**h**) and twf1/twf2-KO cells (**i**). Data represent mean of n=5 cells from one experiment, with standard deviations shown. The '0 μm' value in the x-axis is set to correspond to the peak intensity of phalloidin. **j.** The ratio of CP and F-actin colocalization widths were detected by measuring the width of localization at 50% of maximum intensity. Data points represent measurements from individual cells (n = 20) from two experiments with mean values and standard deviations shown. Statistical source data are provided in Source Data Fig. 4.

Figure 5. Twinfilin regulates capping protein dynamics. **a.** Representative example of fluorescence recovery after photobleaching of EGFP-CP in wild-type and twinfilin-1/twinfilin-2 knockout cells. Scale bars = 5 µm. Bleached regions in the lamellipodia are highlighted with dotted squares. **b.** Analysis of the FRAP experiments. Data represent mean of n=12 measurements on wild-type cells and n=9 measurements on knockout cells from three experiments, and shaded surfaces represent standard deviations. Halftimes of EGFP-CP fluorescence recoveries were: B16-F1 wt = 2.295 s, twf1/twf2-KO = 30.35 s. **c.** Representative examples of fluorescence recovery after photobleaching experiment on wild-type, and **d.** twf1/twf2-KO cells expressing EGFP-CP (cyan) and mCherry-LifeAct (magenta). The recovery of EGFP-CP fluorescence was measured from LifeAct-positive endosomal EGFP-CP puncta. Scale bars = 10 µm. Regions of interest are highlighted with white squares and magnified in panels on right with indicated time points. **e.** Recovery of EGFP-CP fluorescence over time in wild-type and twf1/twf2-KO cells. Each data point represents the mean of n=8 and n=9 individual measurements from three experiments, respectively, with shaded surfaces indicating standard deviations. Halftimes of EGFP-CP fluorescence recoveries were 2.30 s (bound fraction) and 0.45 s (diffuse fraction) for wild type cells, and 18.21 s (bound fraction) and 1.03 s (diffuse fraction) for twf1/twf2-KO cells. Statistical source data are provided in Source Data Fig. 5.

Figure 6. Twinfilin accelerates filament barbed end uncapping *in vitro*. **a.** A schematic overview on the *in vitro* single filament experimental approach. **b.** Filament uncapping at different Twf1 concentrations. Following label order, n = 480, 60, 60, 170, 300, 181 filaments from N = 8, 1, 1, 3, 5, 5 experiments. Fraction of uncapped filament barbed ends are shown with line graph. **c.** V-1 with Twf1, but not V-1 alone, further accelerates uncapping. Following label order, n = 480, 180, 300, 241 filaments from N = 8, 3, 5, 4 experiments. Fraction of uncapped filament barbed ends are shown as thick lines with 95% confidence intervals shown as shaded surfaces and with single exponential fits as thin lines. We measured the off-rates for CP at barbed ends to be 0.13 $x10^{-3}$ s^{-1} in buffer control, 0.8 $x10^{-3}$ s^{-1} in

presence of twinfilin-1, 0.2 x10^{-3} s^{-1} in presence of V-1, and 6.7 x10^{-3} s^{-1} in presence of both twinfilin-1 and V-1. Statistical source data are provided in Source Data Fig. 6.

Figure 7. The actin-binding function of twinfilin is required for filament uncapping. a. Twinfilin-1 mutants used in this study. TWF-1 tail mutant (F323A, K325A, K327A) does not interact with CP, and has decreased affinity for phosphoinositides[42], TWF-1 domain mutant (R96A, K98A, R267A, R269A) does not interact with actin[48,65]. **b.** Twf1 domain mutant, but not Twf1 tail mutant, fails to accelerate CP unbinding *in vitro*. Following label order, n = 480, 120, 181, 240 filaments. Thin grey lines are single exponential fits Fraction of uncapped filament barbed ends are shown as thick lines with 95% confidence intervals shown as shaded surfaces and with single exponential fits as thin lines. **c.** FRAP of EGFP-CP in twf1/twf2-KO cells expressing wild-type mCherry-TWF-1, mCherry-TWF-1 tail mutant, or mCherry-TWF-1 domain mutant. Timepoint "Pre" is a frame before bleaching with a region of bleaching indicated with a dotted square, and 0 s the first frame after the bleaching. Scale bars = 5 µm. **d.** Analysis of fluorescence recovery of EGFP-CP. Data represent mean of n=14, n=13, and n=8 measurements from N=2, N=3, and N=2 experiments on mCherry-TWF1-wt, mCherry-TWF1-tail mutant, and mCherry-TWF1-domain mutant rescue cells, respectively, with shaded surfaces representing standard deviations. Halftimes of recoveries for EGFP-CP in cells expressing different mCherry-tagged proteins: mCherry-TWF-1 wild-type = 1.3 s, mCherry-TWF-1 tail mutant = 9.2 s, mCherry-TWF-1 domain mutant = 25.5 s. Statistical source data are provided in Source Data Fig. 7.

Figure 8. Localization of twinfilin in lamellipodia and its role in regulation of Capping Protein dynamics. a-b. Examples of localization of EGFP-tagged wild-type twinfilin-1 (**a**) and the tail mutant (F323A, K325A, K327A) (**b**) in B16-F1 cells. Scale bars = 10 µm. **c-d.** Line profile analysis of the wild-type EGFP-twinfilin-1 (**c**) and the tail mutant (**d**) compared to AlexaFluor-568-phalloidin in the lamellipodia of B16-F1 cells. Line profiles were generated from the middle of the lamellipodia, as

indicated with the dotted lines. Data represent mean of n=23 (wild-type twinfilin-1) and n=19 (twinfilin-1 tail mutant) cells from one experiment with standard deviations shown. **e-g.** A working model on how twinfilin regulates capping protein and actin filament dynamics. **e.** Twinfilin dissociates CP from filament barbed end by associating with the filament end. V-1 co-operates with twinfilin to enhance the uncapping rate by dissociating CP from twinfilin. Twinfilin transiently interacts with filament barbed ends to slow down both filament polymerization and depolymerization. **f.** In wild-type cells, CP is loaded to barbed ends of actin filaments by CARMIL or other CPI motif proteins. Twinfilin uncaps aged actin filament barbed ends, and thus promotes CP dynamics and restricts its localization to the distal parts of the lamellipodial actin filament network. Aged actin filaments undergo depolymerization from both ends to maintain polymerization-competent pool of ATP-G-actin. ADF/cofilins decorate aged filaments to promote CP-dissociation, filament severing, barbed end depolymerization and pointed end depolymerization together with cyclase-associated protein. **g.** In the absence of twinfilin, CP more stably caps filament barbed ends throughout the entire lamellipodium. This results in diminished actin filament barbed end depolymerization, and filaments disassemble mostly from their pointed ends. ADF/cofilin can accelerate CP dynamics by severing actin filaments[38] and dissociating CP from barbed ends[35], but its possible synergistic effect on uncapping together with twinfilins remains to be studied. Statistical source data are provided in Source Data Fig. 8.

Figure 1

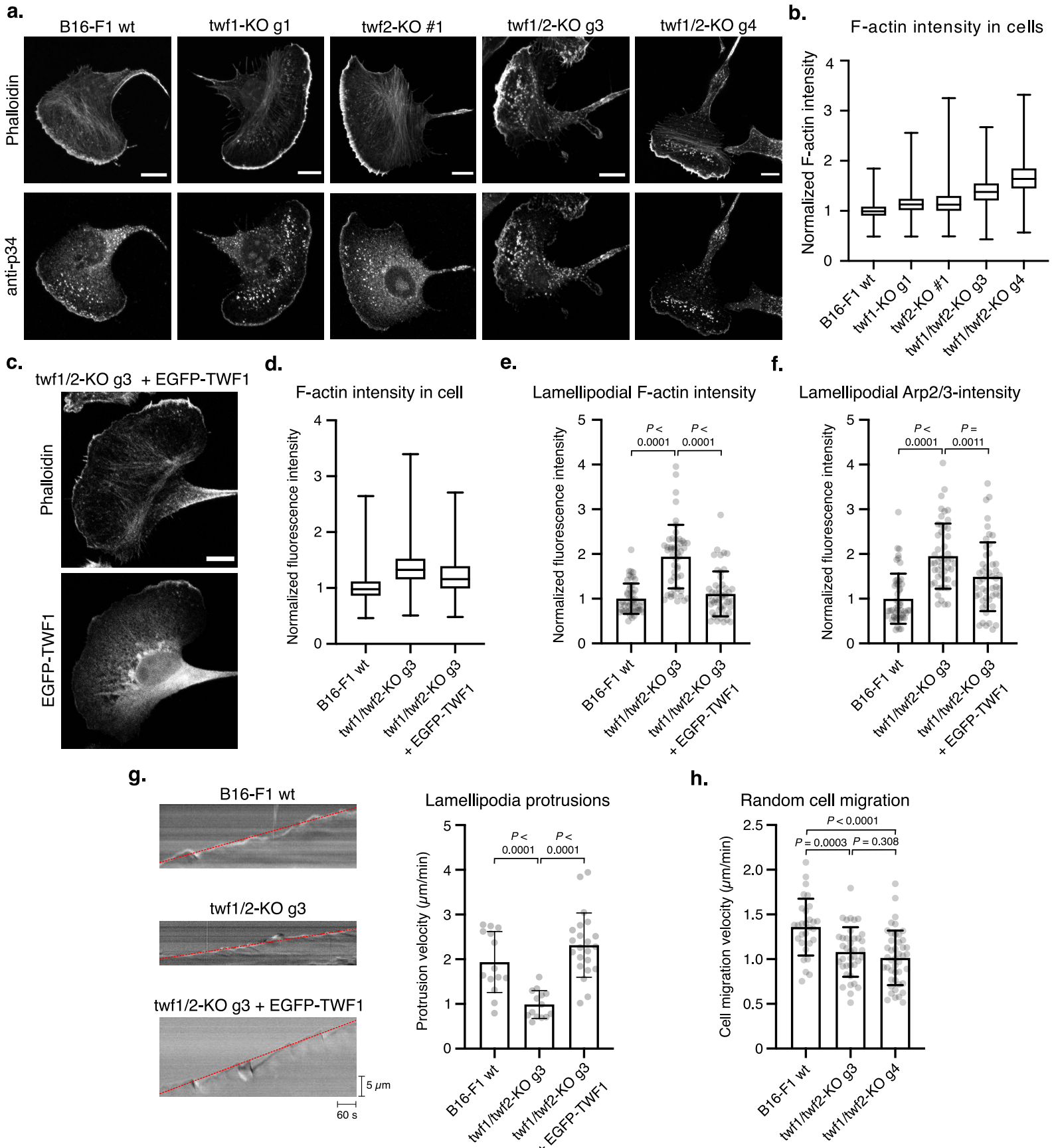
a.
B16-F1 wt
twf1-KO g1
twf2-KO #1
twf1/2-KO g3
twf1/2-KO g4
Phalloidin
anti-p34
b.
F-actin intensity in cells
Normalized F-actin intensity
B16-F1 wt
twf1-KO g1
twf2-KO #1
twf1/twf2-KO g3
twf1/twf2-KO g4
c.
twf1/2-KO g3 + EGFP-TWF1
Phalloidin
EGFP-TWF1
d.
F-actin intensity in cell
Normalized fluorescence intensity
B16-F1 wt
twf1/twf2-KO g3
twf1/twf2-KO g3 + EGFP-TWF1
e.
Lamellipodial F-actin intensity
Normalized fluorescence intensity
P < 0.0001
P < 0.0001
f.
Lamellipodial Arp2/3-intensity
Normalized fluorescence intensity
P < 0.0001
P = 0.0011
g.
B16-F1 wt
twf1/2-KO g3
twf1/2-KO g3 + EGFP-TWF1
5 µm
60 s
Lamellipodia protrusions
Protrusion velocity (µm/min)
P < 0.0001
P < 0.0001
h.
Random cell migration
Cell migration velocity (µm/min)
P < 0.0001
P = 0.0003
P = 0.308
B16-F1 wt
twf1/twf2-KO g3
twf1/twf2-KO g4

Figure 2

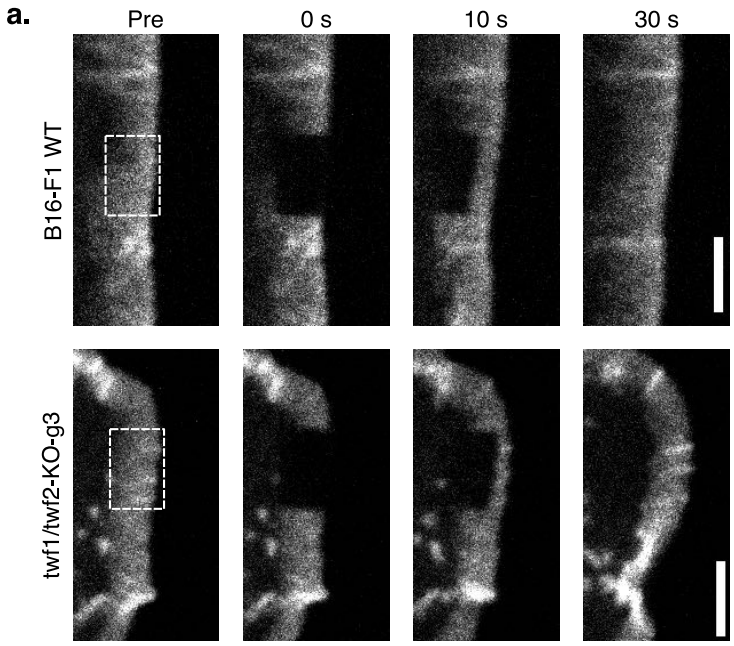
a.
Pre
0 s
10 s
30 s
B16-F1 WT
twf1/twf2-KO-g3

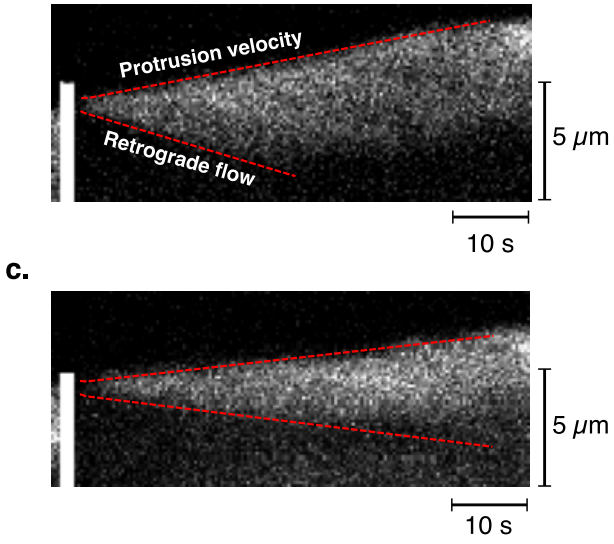
b.
Protrusion velocity
Retrograde flow
5 μm
10 s
c.
5 μm
10 s

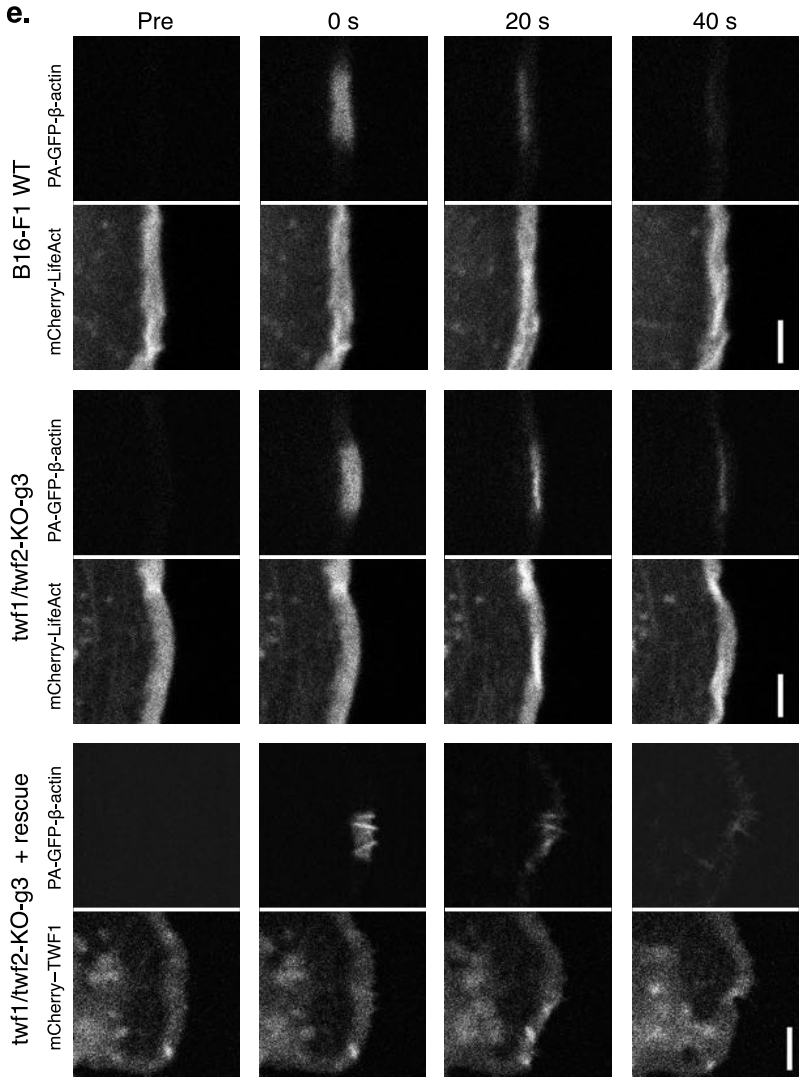
e.
Pre
0 s
20 s
40 s
B16-F1 WT
PA-GFP-β-actin
mCherry-LifeAct
twf1/twf2-KO-g3
PA-GFP-β-actin
mCherry-LifeAct
twf1/twf2-KO-g3 + rescue
PA-GFP-β-actin
mCherry–TWF1

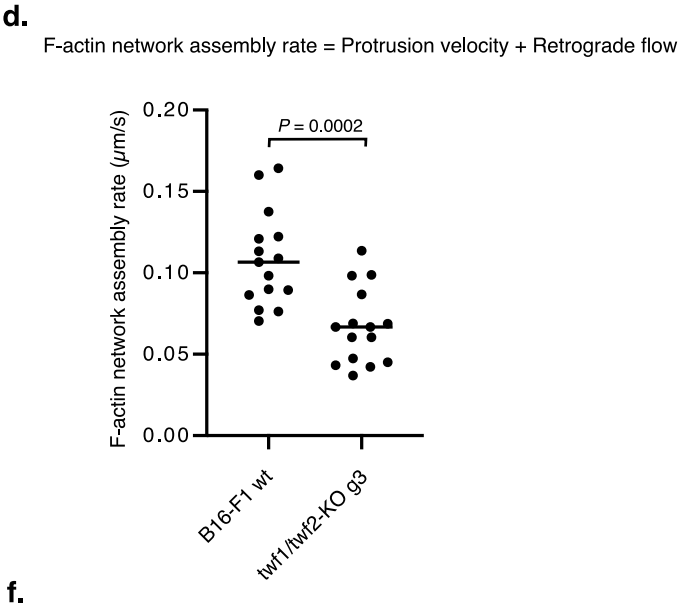
d.
F-actin network assembly rate = Protrusion velocity + Retrograde flow
F-actin network assembly rate (μm/s)
0.20
0.15
0.10
0.05
0.00
P = 0.0002
B16-F1 wt
twf1/twf2-KO g3

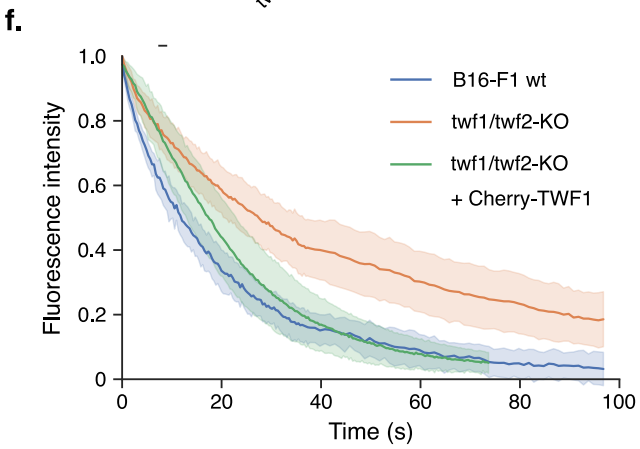
f.
Fluorescence intensity
1.0
0.8
0.6
0.4
0.2
0
0
20
40
60
80
100
Time (s)
B16-F1 wt
twf1/twf2-KO
twf1/twf2-KO
+ Cherry-TWF1

Figure 3

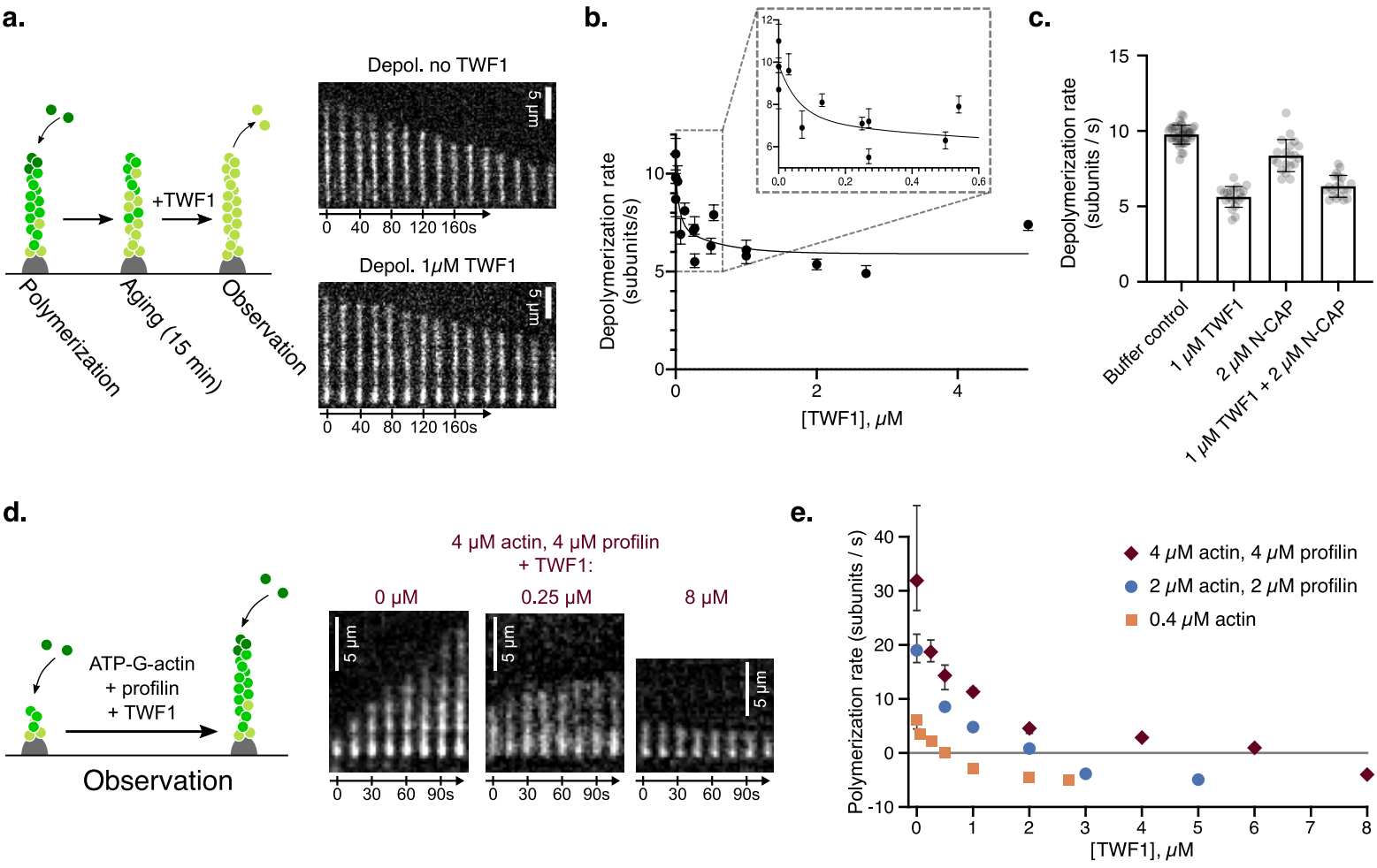
a.
+TWF1
Polymerization
Aging (15 min)
Observation
Depol. no TWF1
5 µm
0 40 80 120 160s
Depol. 1µM TWF1
5 µm
0 40 80 120 160s
b.
Depolymerization rate (subunits/s)
[TWF1], µM
c.
Depolymerization rate (subunits / s)
Buffer control
1 µM TWF1
2 µM N-CAP
1 µM TWF1 + 2 µM N-CAP
d.
ATP-G-actin
+ profilin
+ TWF1
Observation
4 µM actin, 4 µM profilin
+ TWF1:
0 µM
0.25 µM
8 µM
5 µm
0 30 60 90s
e.
Polymerization rate (subunits / s)
[TWF1], µM
4 µM actin, 4 µM profilin
2 µM actin, 2 µM profilin
0.4 µM actin

Figure 4

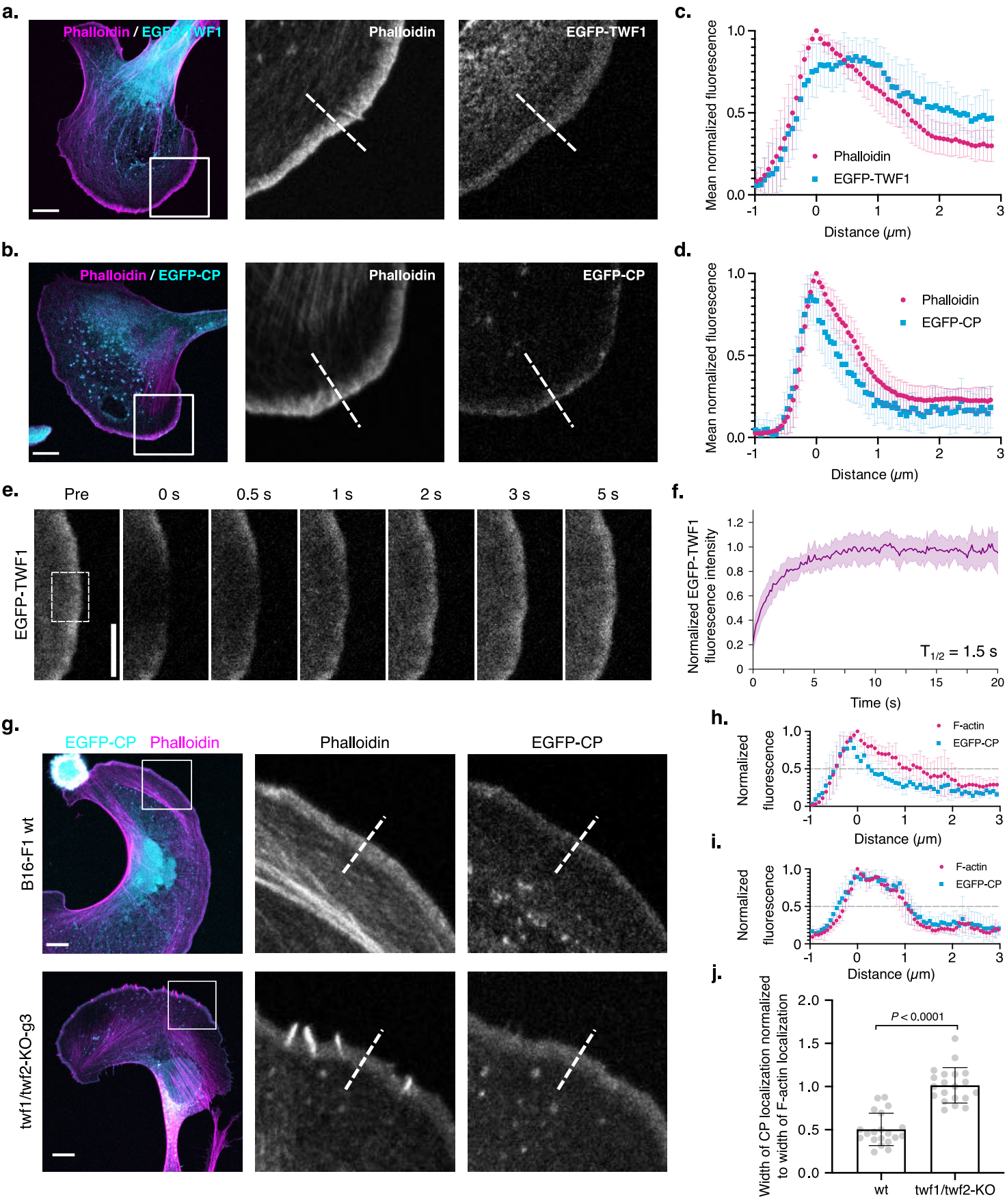
a.
Phalloidin / EGFP-TWF1
Phalloidin
EGFP-TWF1
b.
Phalloidin / EGFP-CP
Phalloidin
EGFP-CP
c.
Mean normalized fluorescence
Phalloidin
EGFP-TWF1
Distance (μm)
d.
Mean normalized fluorescence
Phalloidin
EGFP-CP
Distance (μm)
e.
Pre
0 s
0.5 s
1 s
2 s
3 s
5 s
EGFP-TWF1
f.
Normalized EGFP-TWF1 fluorescence intensity
T1/2 = 1.5 s
Time (s)
g.
EGFP-CP Phalloidin
Phalloidin
EGFP-CP
B16-F1 wt
twf1/twf2-KO-g3
h.
Normalized fluorescence
F-actin
EGFP-CP
Distance (μm)
i.
Normalized fluorescence
F-actin
EGFP-CP
Distance (μm)
j.
Width of CP localization normalized to width of F-actin localization
P < 0.0001
wt
twf1/twf2-KO

Figure 5

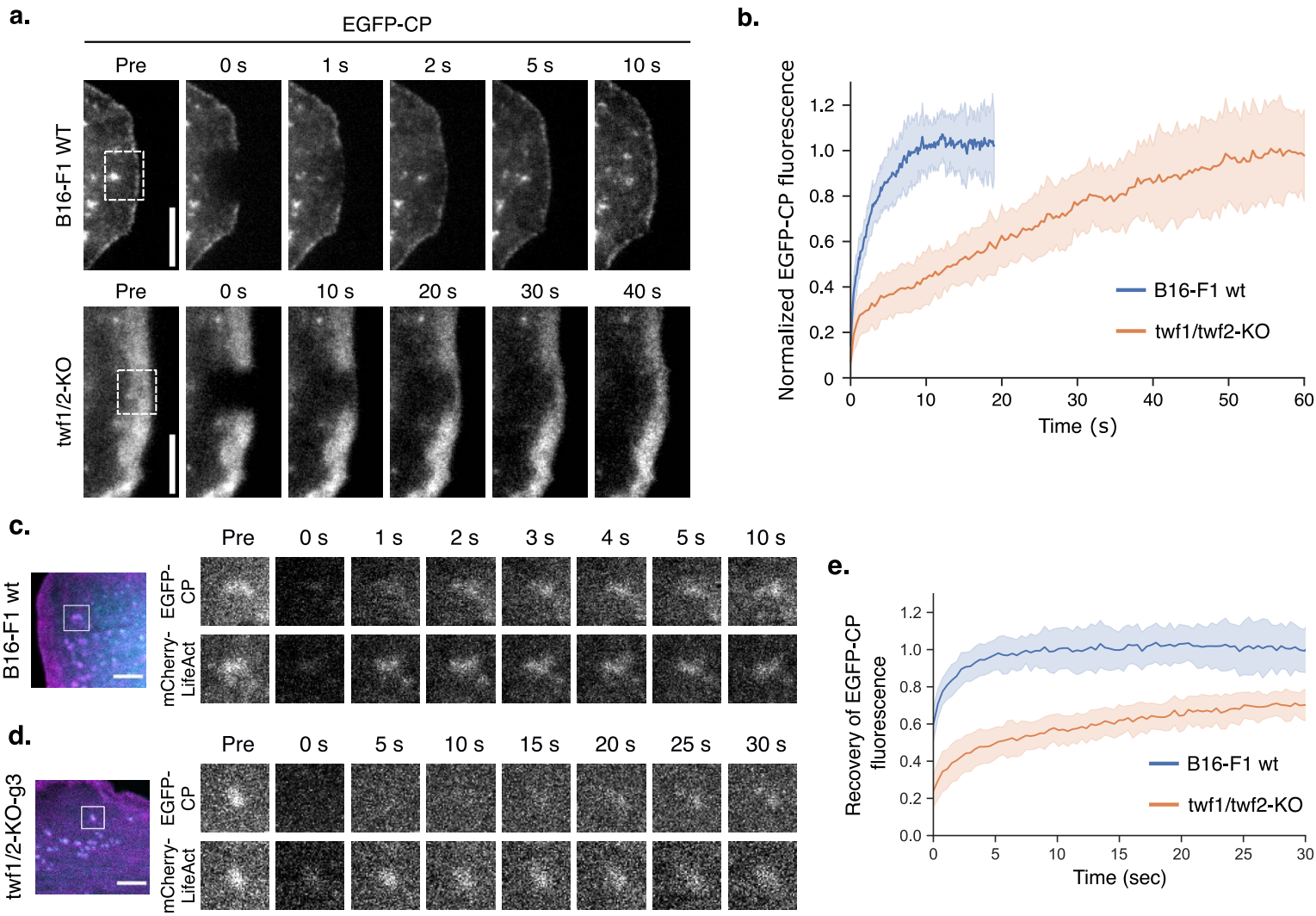
a.
EGFP-CP
Pre
0 s
1 s
2 s
5 s
10 s
B16-F1 WT
Pre
0 s
10 s
20 s
30 s
40 s
twf1/2-KO
b.
Normalized EGFP-CP fluorescence
1.2
1.0
0.8
0.6
0.4
0.2
0
0
10
20
30
40
50
60
Time (s)
B16-F1 wt
twf1/twf2-KO
c.
B16-F1 wt
Pre
0 s
1 s
2 s
3 s
4 s
5 s
10 s
EGFP-CP
mCherry-LifeAct
d.
twf1/2-KO-g3
Pre
0 s
5 s
10 s
15 s
20 s
25 s
30 s
EGFP-CP
mCherry-LifeAct
e.
Recovery of EGFP-CP fluorescence
1.2
1.0
0.8
0.6
0.4
0.2
0.0
0
5
10
15
20
25
30
Time (sec)
B16-F1 wt
twf1/twf2-KO

Figure 6

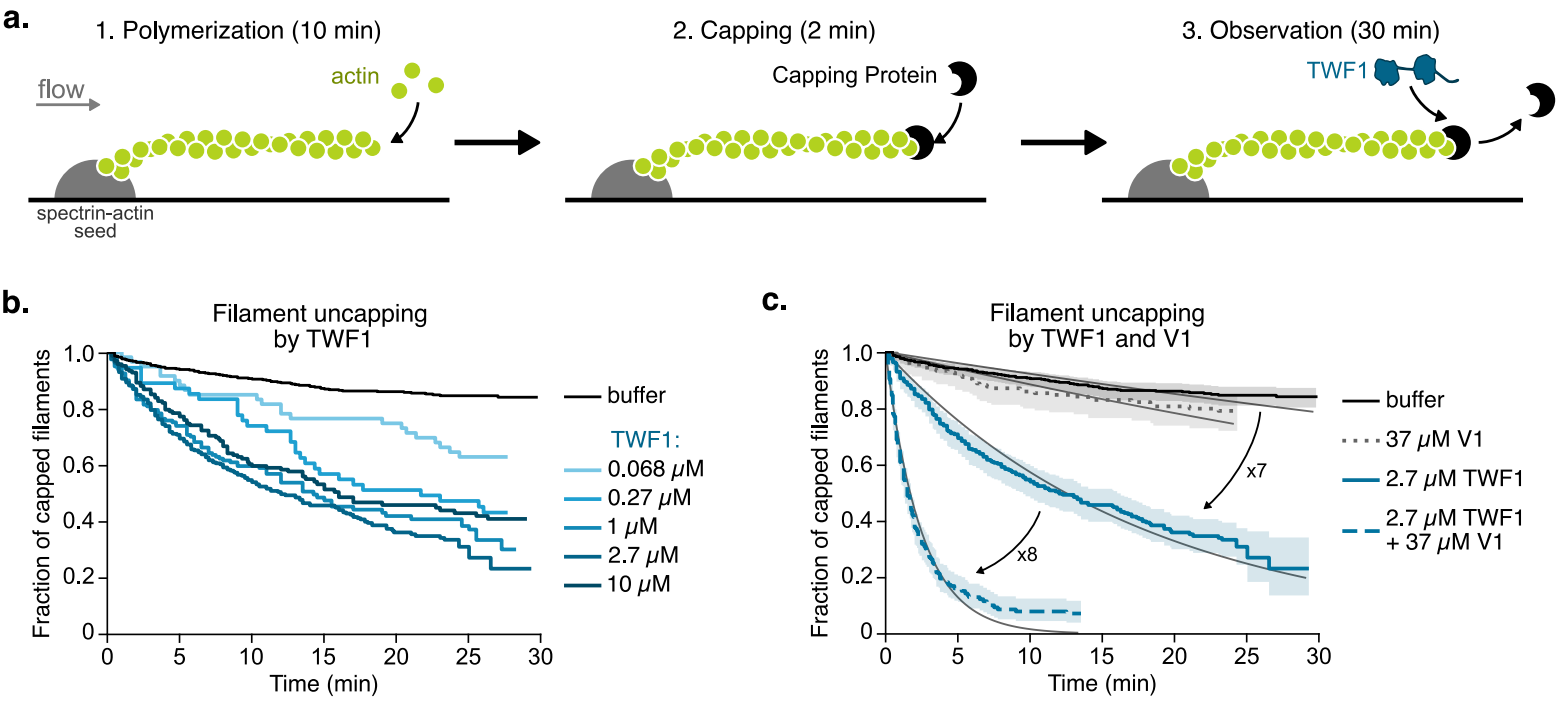
a.
1. Polymerization (10 min)
2. Capping (2 min)
3. Observation (30 min)
flow
actin
Capping Protein
TWF1
spectrin-actin seed
b.
Filament uncapping by TWF1
Fraction of capped filaments
Time (min)
buffer
TWF1:
0.068 μM
0.27 μM
1 μM
2.7 μM
10 μM
c.
Filament uncapping by TWF1 and V1
Fraction of capped filaments
Time (min)
x7
x8
buffer
37 μM V1
2.7 μM TWF1
2.7 μM TWF1 + 37 μM V1

Figure 7

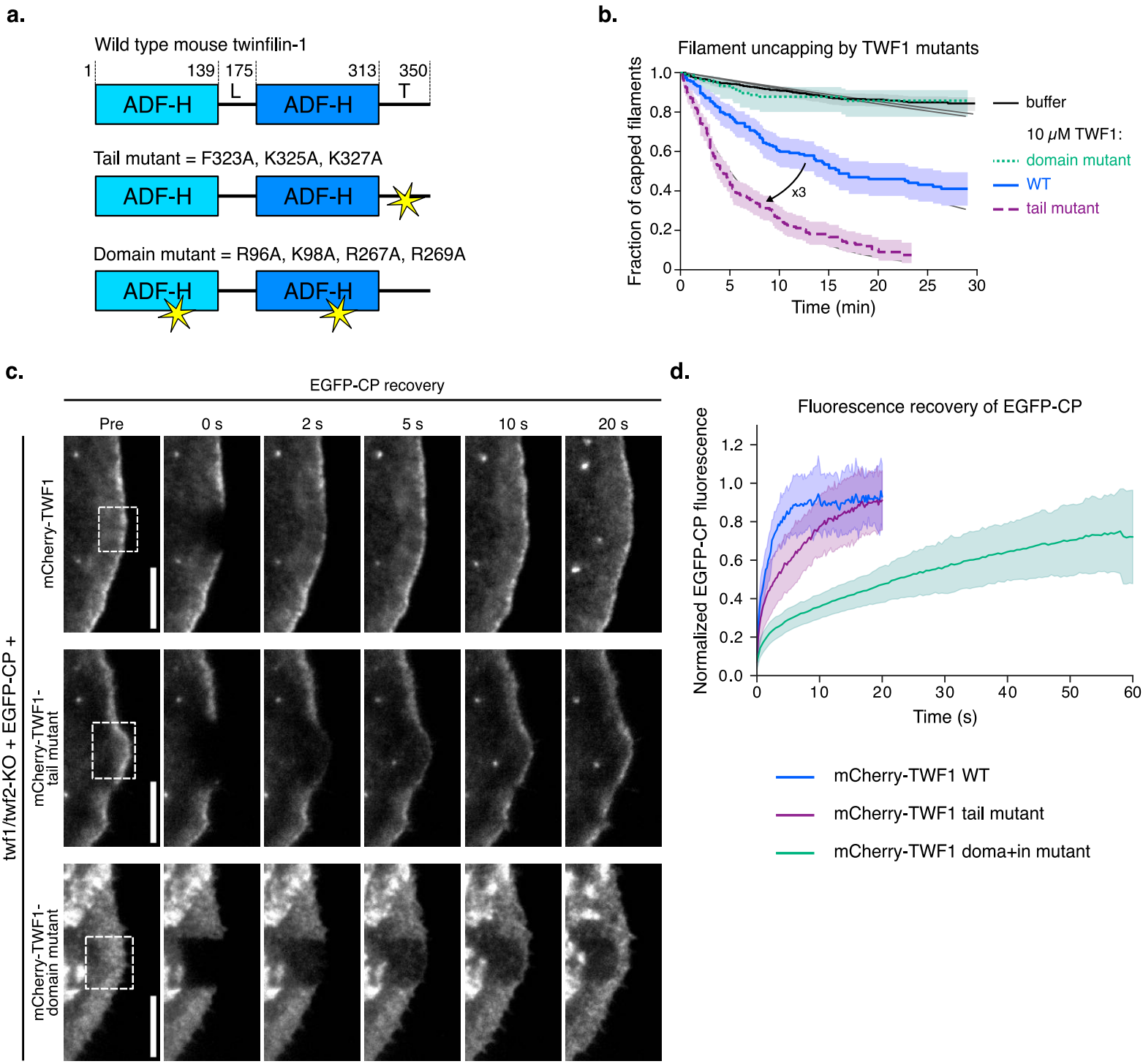
a.
Wild type mouse twinfilin-1
1
139
175
313
350
ADF-H
L
ADF-H
T
Tail mutant = F323A, K325A, K327A
ADF-H
ADF-H
Domain mutant = R96A, K98A, R267A, R269A
ADF-H
ADF-H
b.
Filament uncapping by TWF1 mutants
Fraction of capped filaments
Time (min)
x3
buffer
10 μM TWF1:
domain mutant
WT
tail mutant
c.
EGFP-CP recovery
Pre
0 s
2 s
5 s
10 s
20 s
twf1/twf2-KO + EGFP-CP +
mCherry-TWF1
mCherry-TWF1-tail mutant
mCherry-TWF1-domain mutant
d.
Fluorescence recovery of EGFP-CP
Normalized EGFP-CP fluorescence
Time (s)
mCherry-TWF1 WT
mCherry-TWF1 tail mutant
mCherry-TWF1 doma+in mutant

Figure 8

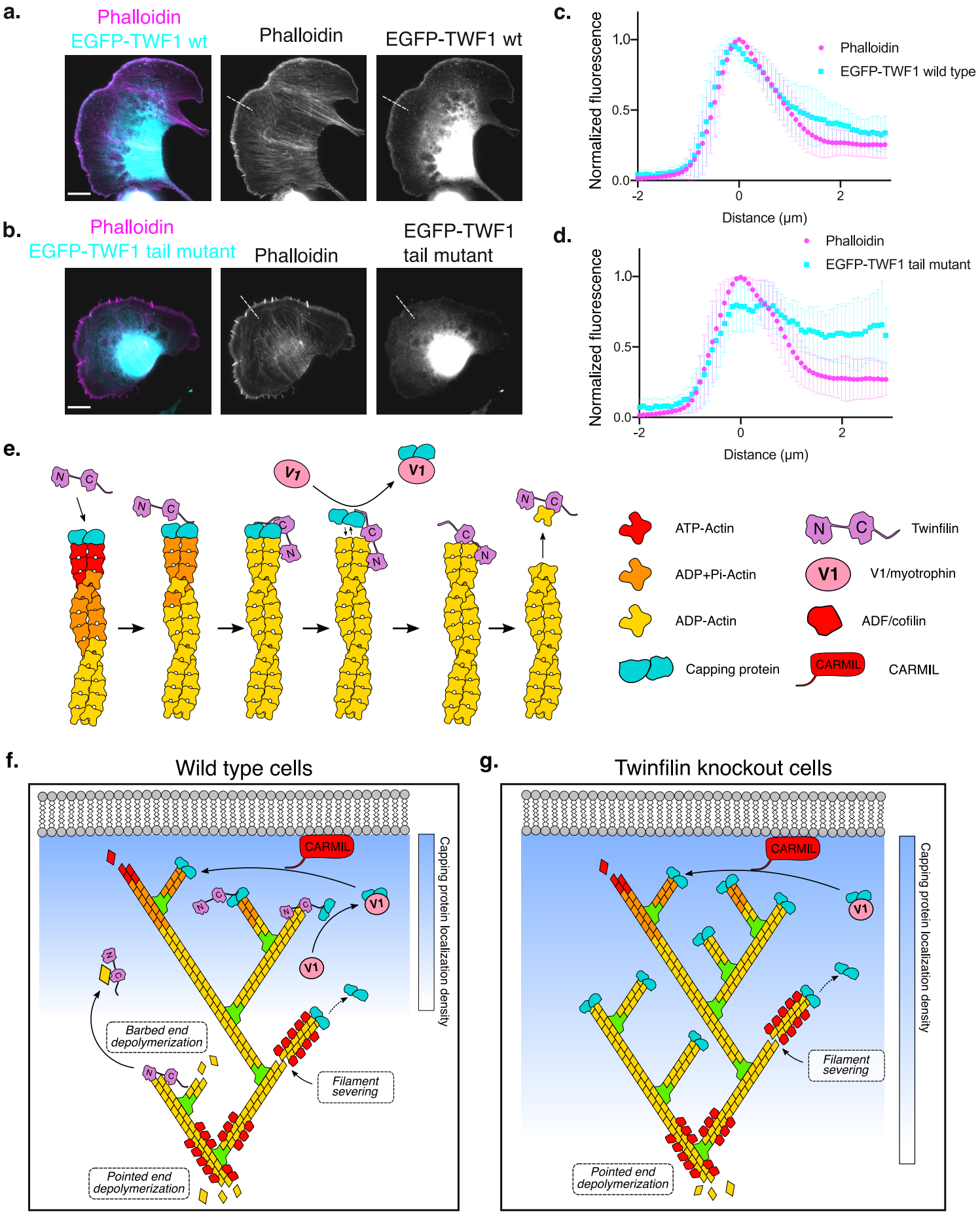
a.
Phalloidin
EGFP-TWF1 wt
Phalloidin
EGFP-TWF1 wt
b.
Phalloidin
EGFP-TWF1 tail mutant
Phalloidin
EGFP-TWF1
tail mutant
c.
Normalized fluorescence
1.0
0.5
0.0
-2
0
2
Distance (μm)
Phalloidin
EGFP-TWF1 wild type
d.
Normalized fluorescence
1.0
0.5
0.0
-2
0
2
Distance (μm)
Phalloidin
EGFP-TWF1 tail mutant
e.
V1
V1
ATP-Actin
ADP+Pi-Actin
ADP-Actin
Capping protein
Twinfilin
V1/myotrophin
ADF/cofilin
CARMIL
CARMIL
f.
Wild type cells
CARMIL
V1
V1
Barbed end
depolymerization
Filament
severing
Pointed end
depolymerization
Capping protein localization density
g.
Twinfilin knockout cells
CARMIL
V1
Filament
severing
Pointed end
depolymerization
Capping protein localization density

Extended data figure 1

a.

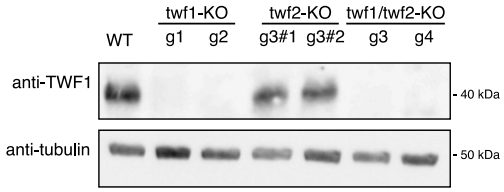

b.

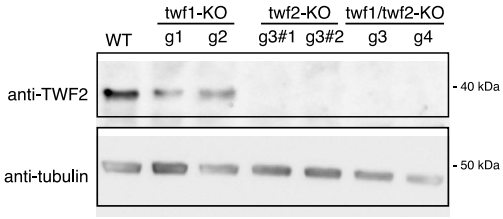

c.

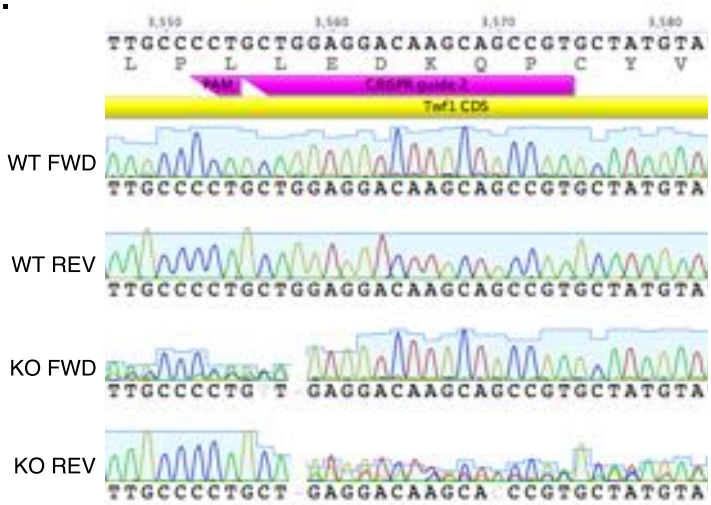

d.

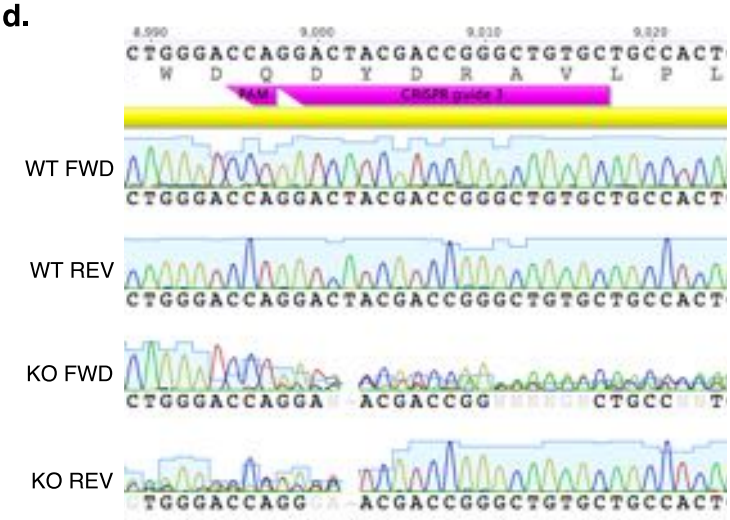

e.

	Sequence: chromosome 15	**Variant frequenzy**	**Translate**
twf-1 wt exon-3	3,547-TTGTCTTGCCCCTGCT–GGAGGACAAGCAG	100%	56-FVLPLLEDKQPCYVLFRLDSQNAQGYEWIFIAWSPDHS
twf-1 KO variant 1	3,547-TTGTCTTGCCCCTGCTTGGAGGACAAGCAG	~66%	56-FVLPLLGGQAAVLCIIQVRLSECPGI-STOP-MDIHCMVS
twf-1 KO variant 2	3,547-TTGTCTTGCCCCTGCT– –GAGGACAAGCAG	~34%	56-FVLPLLRTSSRAMYYSG-STOP-TLRMPRDMNGYSLHG

f.

	Sequence: chromosome 9	**Variant frequenzy**	**Translate**
twf-2 wt exon-3	8,985-GACGCTGGGACCAGGACTACGACCGGGCTG	100%	41-SQEPVGRWDQDYDRAVLPLLDAQEPCYLLFRLDSQNA
twf-2 KO variant 1	8,985-GACGCTGGGACCAGG–CTACGACCGGGCTG	~25%	41-SQEPVGRWDQATTGLCCHC-STOP-TPKSPATSSSDLIR
twf-2 KO variant 2	8,985-GACGCTGGGACCAGGAC–ACGACCGGGCTG	~25%	41-SQEPVGRWDQATTGLCCHC-STOP-TPKSPATSSSDLIR
twf-2 KO variant 3	8,985-GACGCTGGGACCAGGA––ACGACCGGGCTG	~25%	41-SQEPVGRWDQERPGCAATARRPRALLPPLPT-STOP-FA
twf-2 KO variant 4	8,985-GACGCTGGGACCA–––––ACGACCGGGCTG	~25%	41-SQEPVGRWDQRPGCAATARRPRALLPPLPT-STOP-FAE

Extended data figure 2

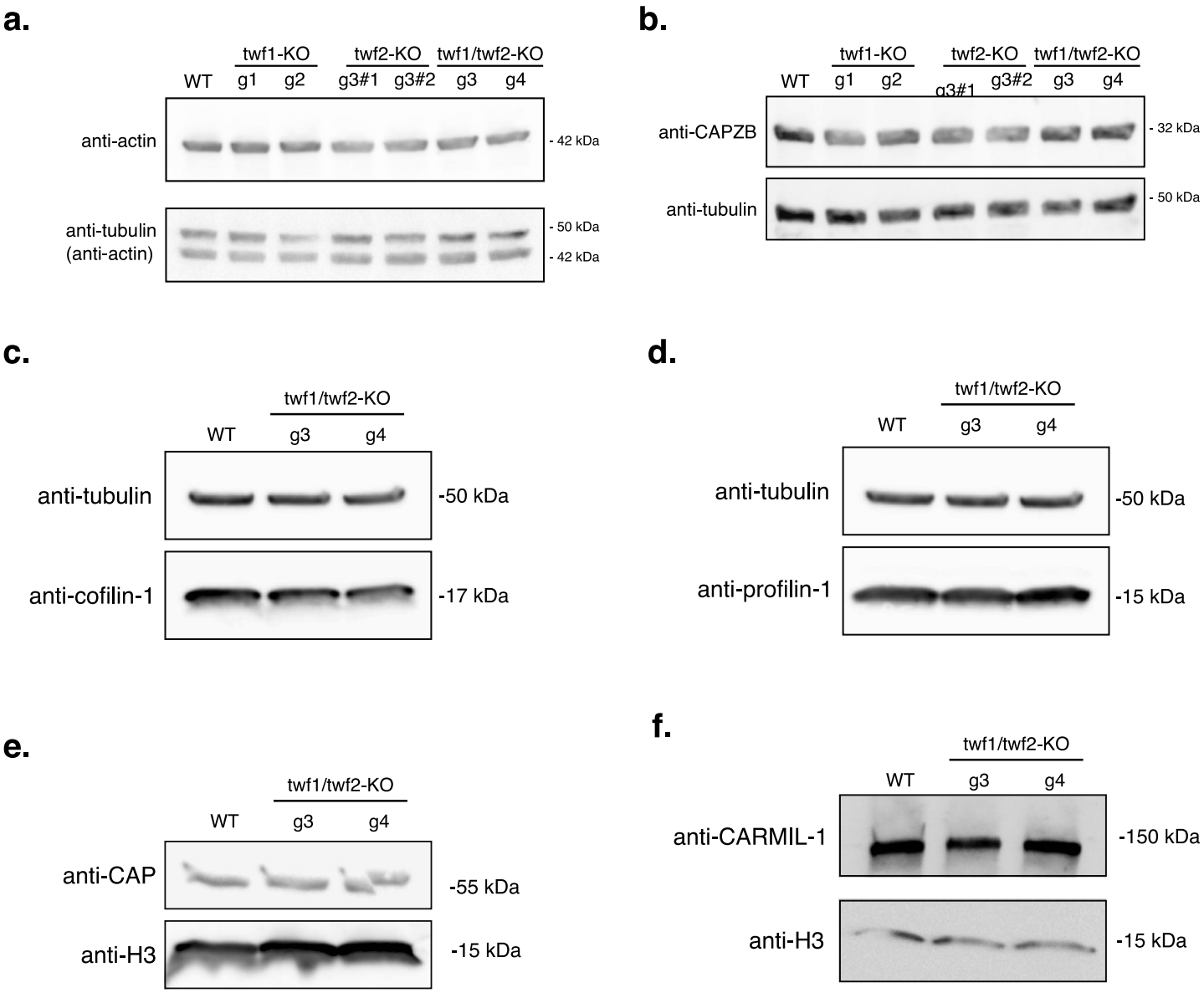

Extended data figure 3

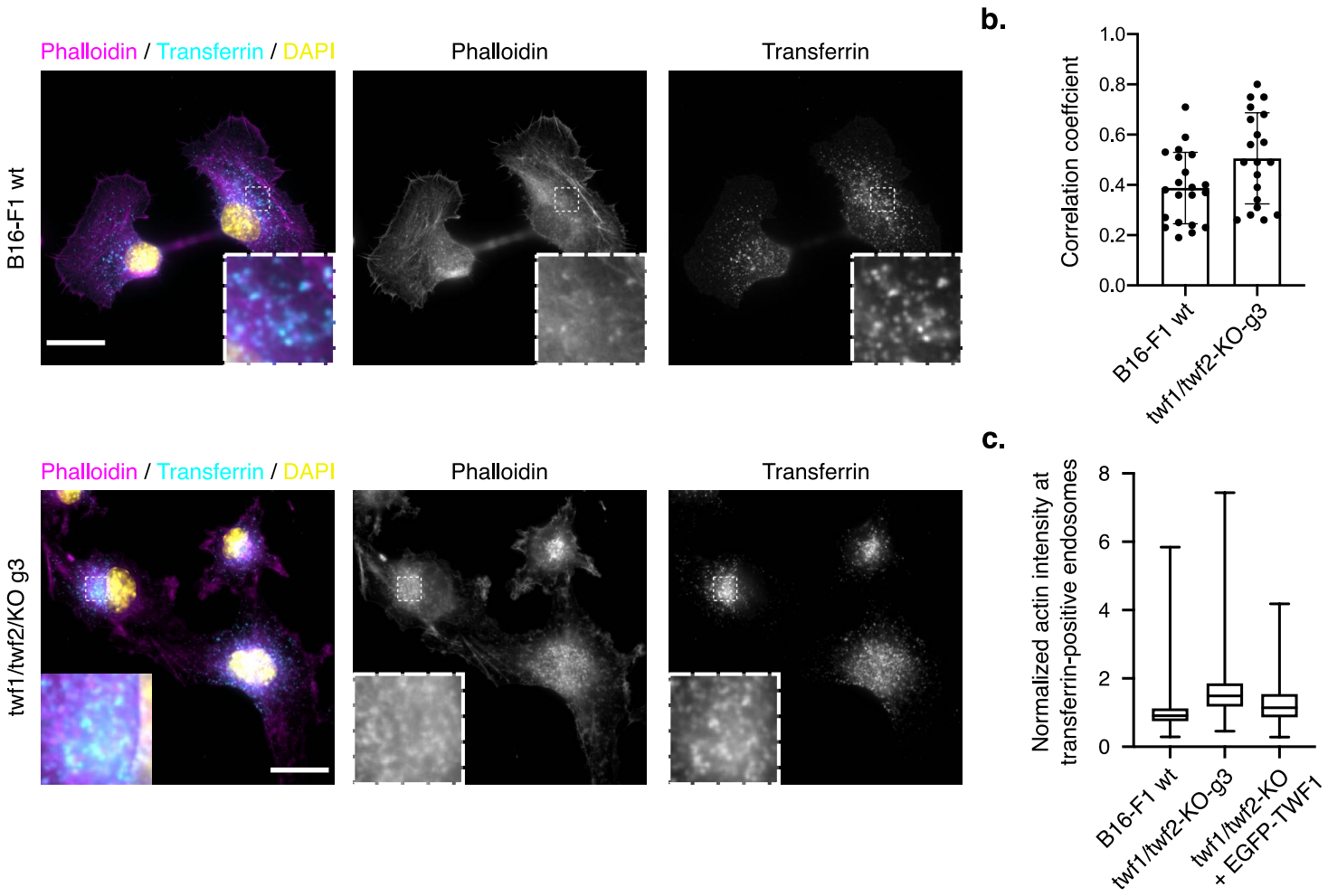

Extended data figure 4

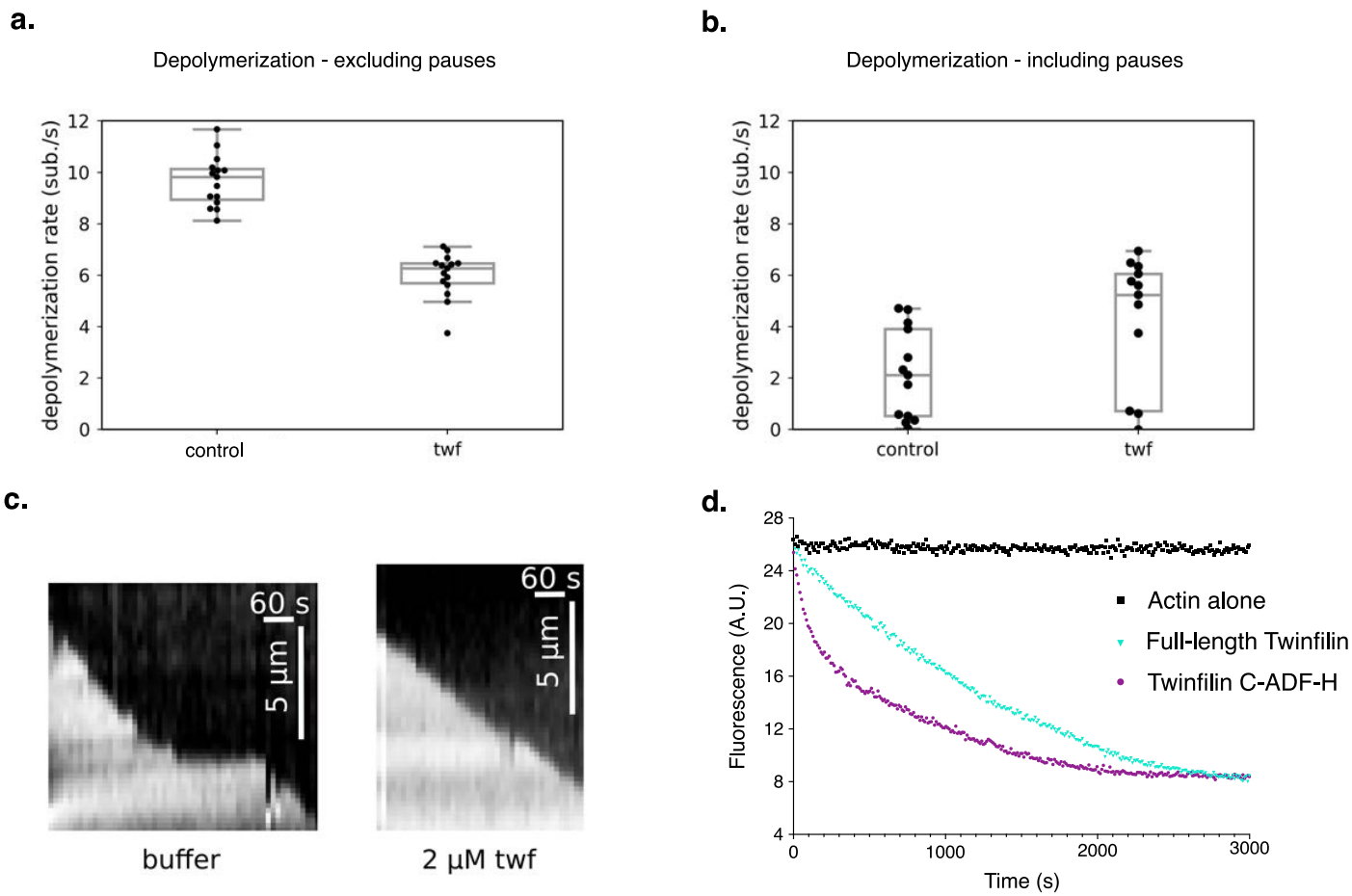

Extended data figure 5

a.

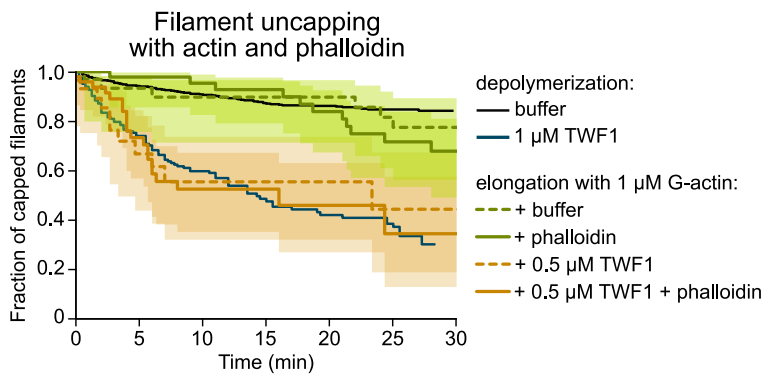

b.

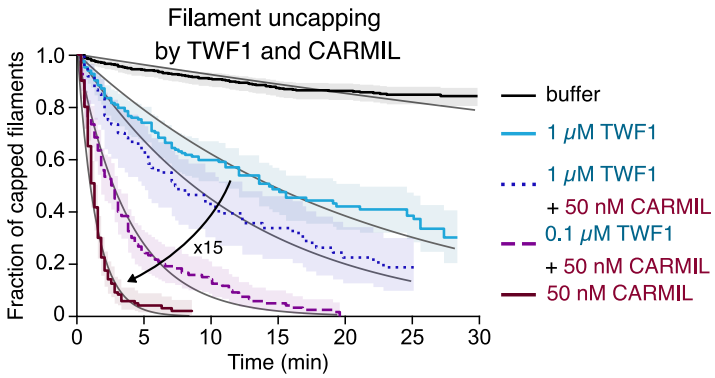

Extended data figure 6

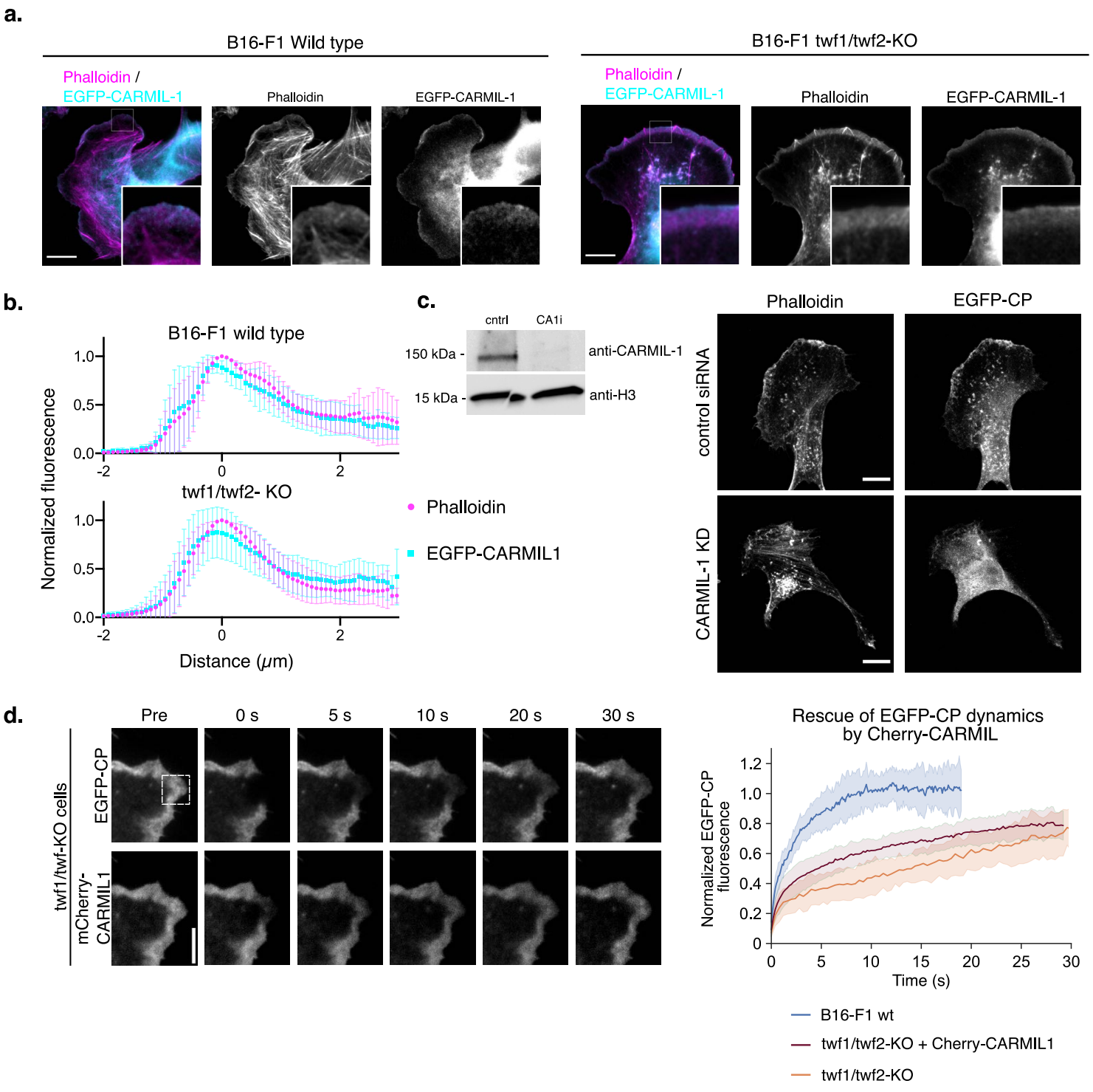

Extended data figure 7

a.

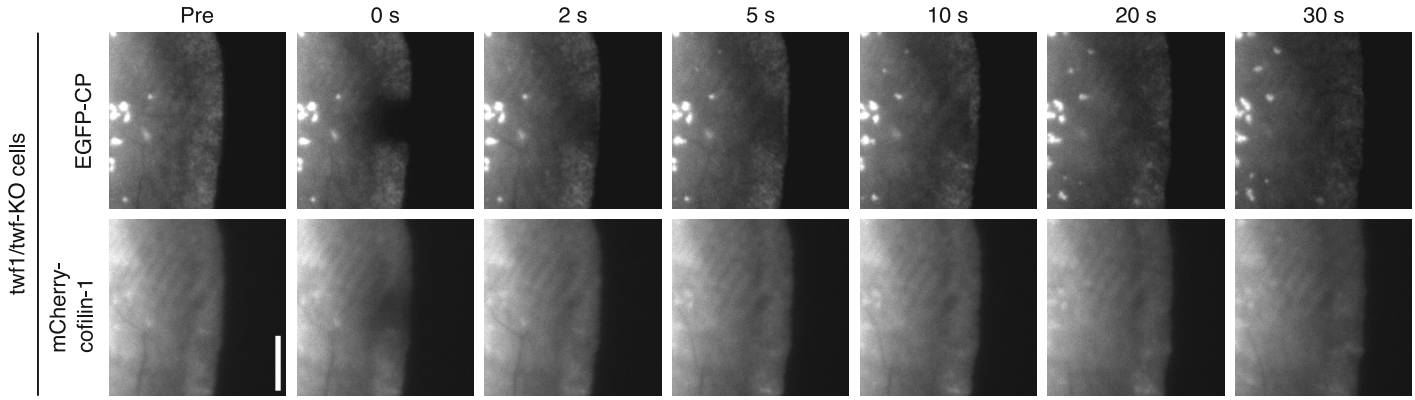

b.

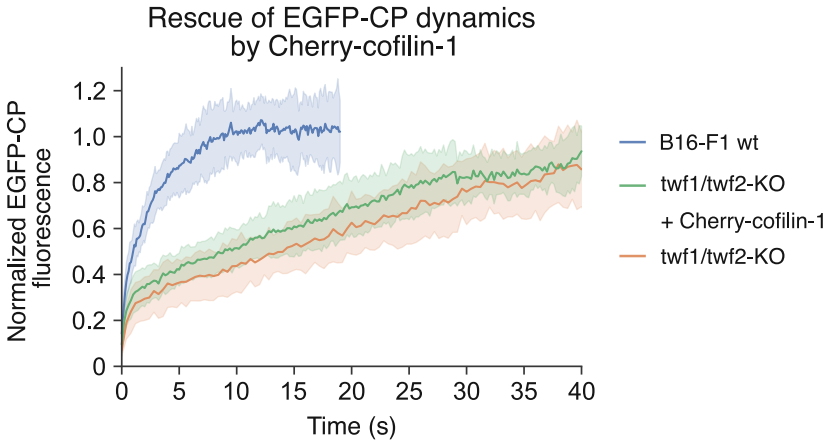

c.

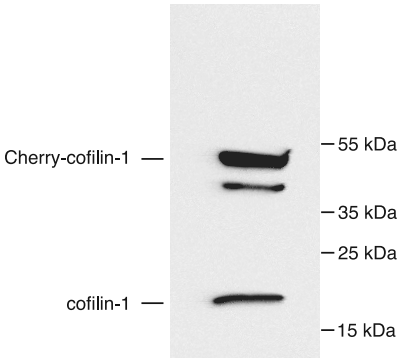

Extended data figure 8

a.

Supplementary figure 1a: Anti-twf1

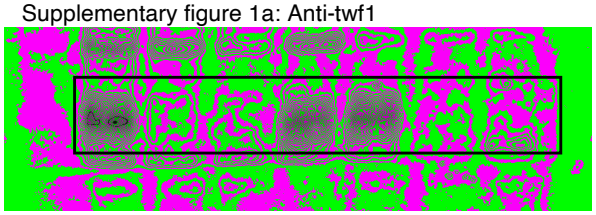

Supplementary figure 1b: Anti-twf2

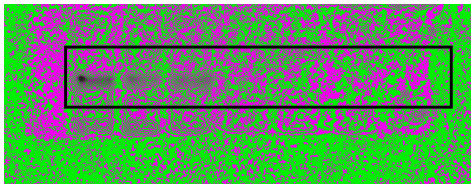

Supplementary figure 1a: Anti-tubulin

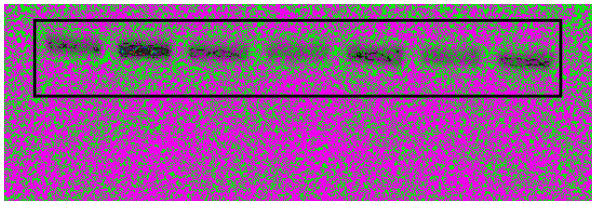

Supplementary figure 1b: Anti-tubulin

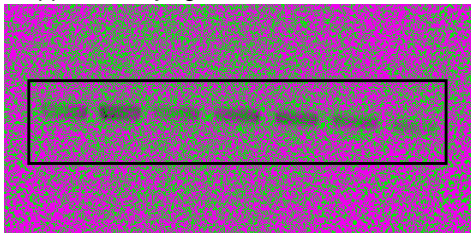

b.

Supplementary figure 3a: anti-actin

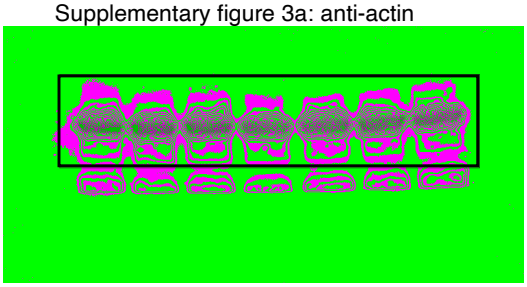

Supplementary figure 3b: anti-CAPZb

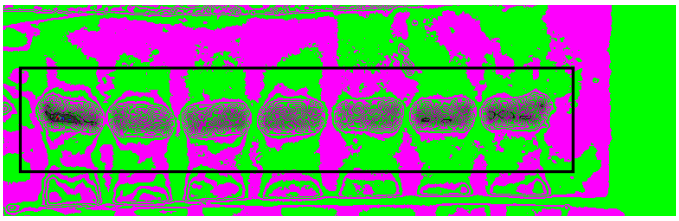

c.

Supplementary figure 3a: anti-tubulin (note that previously blotted anti-actin gives extra band here)

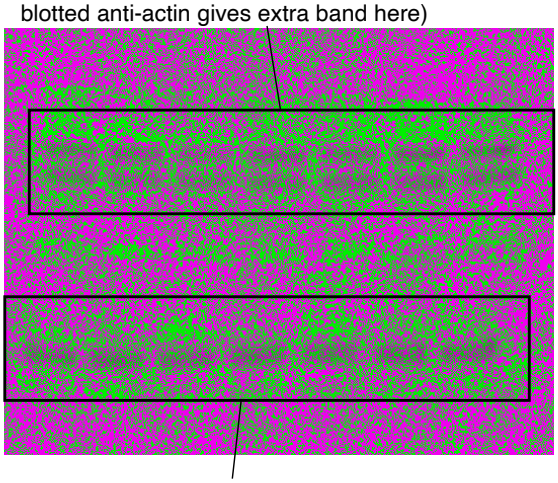

Supplementary figure 3b: anti-tubulin

d.

Supplementary figure 3e: anti-CAP

Supplementary figure 3d: anti-profilin-1

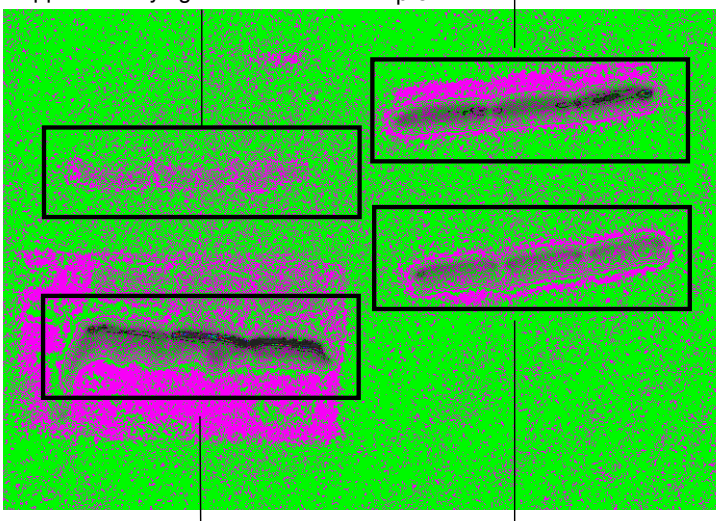

Supplementary figure 3e: anti-H3

Supplementary figure 3c: anti-cofilin-1

e.

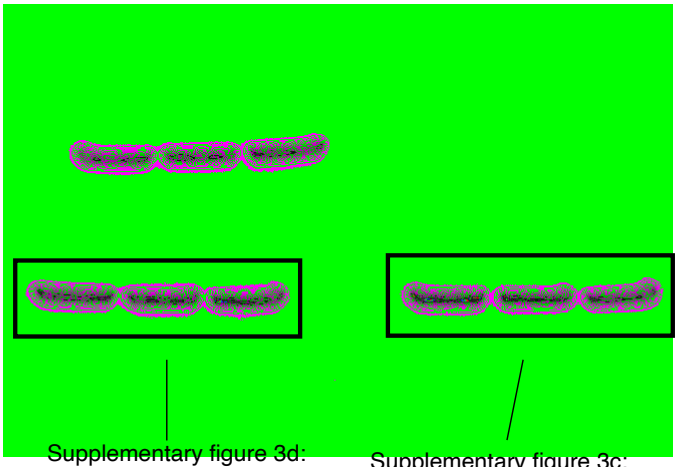

Supplementary figure 3d: anti-tubulin

Supplementary figure 3c: anti-tubulin

Extended data figure 8 (continue)

f.

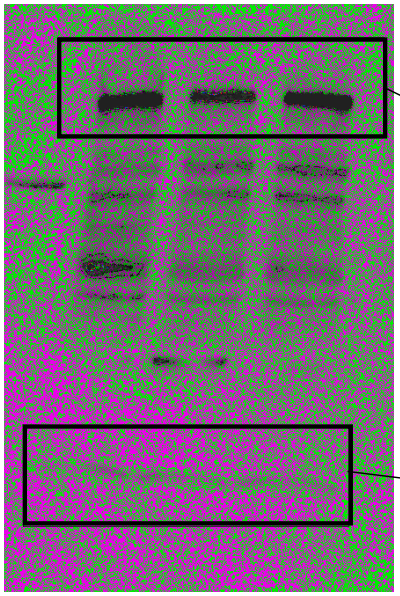

Supplementary figure 3 f: anti-CARMIL1

Supplementary figure 3 f: anti-Histone H3

g.

Supplementary figure 7 e: Anti-CARMIL1

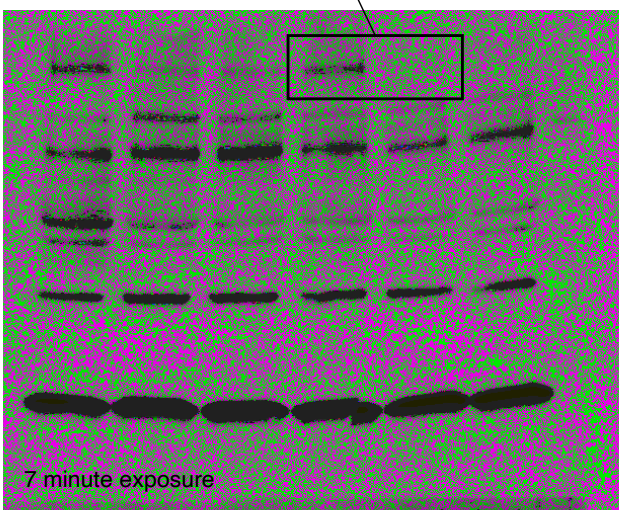

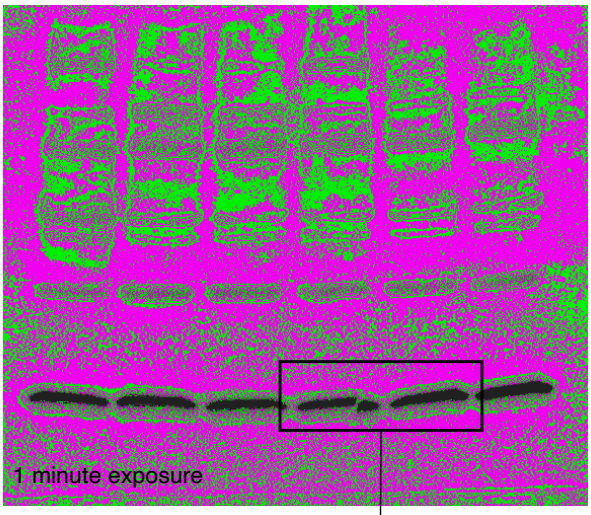

Supplementary figure 7 e: Histone H3

h.

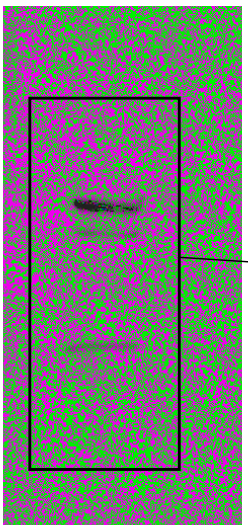

Supplementary fig. 8 c: Anti-cofilin-1 antibody